EUROPEAN LABORATORY FOR PARTICLE PHYSICS

Measurement of the B^+ and B^0 Lifetimes and Search for CP(T) Violation using Reconstructed Secondary Vertices

The OPAL Collaboration

Abstract

The lifetimes of the B^+ and B^0 mesons, and their ratio, have been measured in the OPAL experiment using 2.4 million hadronic Z^0 decays recorded at LEP. $\mathrm{Z}^0 \to \mathrm{b\overline{b}}$ decays were tagged using displaced secondary vertices and high momentum electrons and muons. The lifetimes were then measured using well-reconstructed charged and neutral secondary vertices selected in this tagged data sample. The results are

$$
\begin{aligned}
\tau_{\mathrm{B}^+} &= 1.643 \pm 0.037 \pm 0.025\,\mathrm{ps} \\
\tau_{\mathrm{B}^0} &= 1.523 \pm 0.057 \pm 0.053\,\mathrm{ps} \\
\tau_{\mathrm{B}^+}/\tau_{\mathrm{B}^0} &= 1.079 \pm 0.064 \pm 0.041 \,,
\end{aligned}
$$

where in each case the first error is statistical and the second systematic.

A larger data sample of 3.1 million hadronic Z^0 decays has been used to search for CP and CPT violating effects by comparison of inclusive b and $\overline{\mathrm{b}}$ hadron decays. No evidence for such effects is seen. The CP violation parameter $\mathrm{Re}(\epsilon_\mathrm{B})$ is measured to be

$$
\mathrm{Re}(\epsilon_\mathrm{B}) = 0.001 \pm 0.014 \pm 0.003
$$

and the fractional difference between b and $\overline{\mathrm{b}}$ hadron lifetimes is measured to be

$$
\left(\frac{\Delta\tau}{\tau}\right)_\mathrm{b} \equiv \frac{\tau(\mathrm{b\ hadron}) - \tau(\overline{\mathrm{b}}\ \mathrm{hadron})}{\tau(\mathrm{average})} = -0.001 \pm 0.012 \pm 0.008 \,.
$$

arXiv:hep-ex/9901017v1 13 Jan 1999

The OPAL Collaboration

G. Abbiendi[2], K. Ackerstaff[8], G. Alexander[23], J. Allison[16], N. Altekamp[5], K.J. Anderson[9], S. Anderson[12], S. Arcelli[17], S. Asai[24], S.F. Ashby[1], D. Axen[29], G. Azuelos[18,a], A.H. Ball[17], E. Barberio[8], R.J. Barlow[16], R. Bartoldus[3], J.R. Batley[5], S. Baumann[3], J. Bechtluft[14], T. Behnke[27], K.W. Bell[20], G. Bella[23], A. Bellerive[9], S. Bentvelsen[8], S. Bethke[14], S. Betts[15], O. Biebel[14], A. Biguzzi[5], S.D. Bird[16], V. Blobel[27], I.J. Bloodworth[1], P. Bock[11], J. Böhme[14], D. Bonacorsi[2], M. Boutemeur[34], S. Braibant[8], P. Bright-Thomas[1], L. Brigliadori[2], R.M. Brown[20], H.J. Burckhart[8], P. Capiluppi[2], R.K. Carnegie[6], A.A. Carter[13], J.R. Carter[5], C.Y. Chang[17], D.G. Charlton[1,b], D. Chrisman[4], C. Ciocca[2], P.E.L. Clarke[15], E. Clay[15], I. Cohen[23], J.E. Conboy[15], O.C. Cooke[8], C. Couyoumtzelis[13], R.L. Coxe[9], M. Cuffiani[2], S. Dado[22], G.M. Dallavalle[2], R. Davis[30], S. De Jong[12], A. de Roeck[8], P. Dervan[15], K. Desch[8], B. Dienes[33,d], M.S. Dixit[7], J. Dubbert[34], E. Duchovni[26], G. Duckeck[34], I.P. Duerdoth[16], D. Eatough[16], P.G. Estabrooks[6], E. Etzion[23], F. Fabbri[2], M. Fanti[2], A.A. Faust[30], F. Fiedler[27], M. Fierro[2], I. Fleck[8], R. Folman[26], A. Fürtjes[8], D.I. Futyan[16], P. Gagnon[7], J.W. Gary[4], J. Gascon[18], S.M. Gascon-Shotkin[17], G. Gaycken[27], C. Geich-Gimbel[3], G. Giacomelli[2], P. Giacomelli[2], V. Gibson[5], W.R. Gibson[13], D.M. Gingrich[30,a], D. Glenzinski[9], J. Goldberg[22], W. Gorn[4], C. Grandi[2], K. Graham[28], E. Gross[26], J. Grunhaus[23], M. Gruwé[27], G.G. Hanson[12], M. Hansroul[8], M. Hapke[13], K. Harder[27], A. Harel[22], C.K. Hargrove[7], C. Hartmann[3], M. Hauschild[8], C.M. Hawkes[1], R. Hawkings[27], R.J. Hemingway[6], M. Herndon[17], G. Herten[10], R.D. Heuer[27], M.D. Hildreth[8], J.C. Hill[5], P.R. Hobson[25], M. Hoch[18], A. Hocker[9], K. Hoffman[8], R.J. Homer[1], A.K. Honma[28,a], D. Horváth[32,c], K.R. Hossain[30], R. Howard[29], P. Hüntemeyer[27], P. Igo-Kemenes[11], D.C. Imrie[25], K. Ishii[24], F.R. Jacob[20], A. Jawahery[17], H. Jeremie[18], M. Jimack[1], C.R. Jones[5], P. Jovanovic[1], T.R. Junk[6], D. Karlen[6], V. Kartvelishvili[16], K. Kawagoe[24], T. Kawamoto[24], P.I. Kayal[30], R.K. Keeler[28], R.G. Kellogg[17], B.W. Kennedy[20], D.H. Kim[19], A. Klier[26], S. Kluth[8], T. Kobayashi[24], M. Kobel[3,e], D.S. Koetke[6], T.P. Kokott[3], M. Kolrep[10], S. Komamiya[24], R.V. Kowalewski[28], T. Kress[4], P. Krieger[6], J. von Krogh[11], T. Kuhl[3], P. Kyberd[13], G.D. Lafferty[16], H. Landsman[22], D. Lanske[14], J. Lauber[15], S.R. Lautenschlager[31], I. Lawson[28], J.G. Layter[4], D. Lazic[22], A.M. Lee[31], D. Lellouch[26], J. Letts[12], L. Levinson[26], R. Liebisch[11], B. List[8], C. Littlewood[5], A.W. Lloyd[1], S.L. Lloyd[13], F.K. Loebinger[16], G.D. Long[28], M.J. Losty[7], J. Ludwig[10], D. Liu[12], A. Macchiolo[2], A. Macpherson[30], W. Mader[3], M. Mannelli[8], S. Marcellini[2], C. Markopoulos[13], A.J. Martin[13], J.P. Martin[18], G. Martinez[17], T. Mashimo[24], P. Mättig[26], W.J. McDonald[30], J. McKenna[29], E.A. Mckigney[15], T.J. McMahon[1], R.A. McPherson[28], F. Meijers[8], S. Menke[3], F.S. Merritt[9], H. Mes[7], J. Meyer[27], A. Michelini[2], S. Mihara[24], G. Mikenberg[26], D.J. Miller[15], R. Mir[26], W. Mohr[10], A. Montanari[2], T. Mori[24], K. Nagai[8], I. Nakamura[24], H.A. Neal[12], B. Nellen[3], R. Nisius[8], S.W. O'Neale[1], F.G. Oakham[7], F. Odorici[2], H.O. Ogren[12], M.J. Oreglia[9], S. Orito[24], J. Pálinkás[33,d], G. Pásztor[32], J.R. Pater[16], G.N. Patrick[20], J. Patt[10], R. Perez-Ochoa[8], S. Petzold[27], P. Pfeifenschneider[14], J.E. Pilcher[9], J. Pinfold[30], D.E. Plane[8], P. Poffenberger[28], J. Polok[8], M. Przybycień[8], C. Rembser[8], H. Rick[8], S. Robertson[28], S.A. Robins[22], N. Rodning[30], J.M. Roney[28], K. Roscoe[16], A.M. Rossi[2], Y. Rozen[22], K. Runge[10], O. Runolfsson[8], D.R. Rust[12], K. Sachs[10], T. Saeki[24], O. Sahr[34], W.M. Sang[25], E.K.G. Sarkisyan[23], C. Sbarra[29], A.D. Schaile[34], O. Schaile[34], F. Scharf[3], P. Scharff-Hansen[8], J. Schieck[11], B. Schmitt[8], S. Schmitt[11], A. Schöning[8], M. Schröder[8], M. Schumacher[3], C. Schwick[8], W.G. Scott[20], R. Seuster[14], T.G. Shears[8], B.C. Shen[4], C.H. Shepherd-Themistocleous[8], P. Sherwood[15], G.P. Siroli[2], A. Sittler[27], A. Skuja[17], A.M. Smith[8], G.A. Snow[17], R. Sobie[28], S. Söldner-Rembold[10], S. Spagnolo[20], M. Sproston[20], A. Stahl[3], K. Stephens[16], J. Steuerer[27], K. Stoll[10], D. Strom[19], R. Ströhmer[34], B. Surrow[8], S.D. Talbot[1], S. Tanaka[24], P. Taras[18], S. Tarem[22], R. Teuscher[8], M. Thiergen[10], J. Thomas[15], M.A. Thomson[8], E. von Törne[3], E. Torrence[8], S. Towers[6], I. Trigger[18], Z. Trócsányi[33], E. Tsur[23], A.S. Turcot[9], M.F. Turner-Watson[1], I. Ueda[24], R. Van Kooten[12], P. Vannerem[10], M. Verzocchi[10], H. Voss[3], F. Wäckerle[10], A. Wagner[27], C.P. Ward[5], D.R. Ward[5], P.M. Watkins[1], A.T. Watson[1], N.K. Watson[1], P.S. Wells[8], N. Wermes[3], J.S. White[6], G.W. Wilson[16], J.A. Wilson[1], T.R. Wyatt[16], S. Yamashita[24], G. Yekutieli[26], V. Zacek[18], D. Zer-Zion[8]

[1]School of Physics and Astronomy, University of Birmingham, Birmingham B15 2TT, UK

[2]Dipartimento di Fisica dell' Università di Bologna and INFN, I-40126 Bologna, Italy

[3]Physikalisches Institut, Universität Bonn, D-53115 Bonn, Germany

[4]Department of Physics, University of California, Riverside CA 92521, USA

[5]Cavendish Laboratory, Cambridge CB3 0HE, UK

[6]Ottawa-Carleton Institute for Physics, Department of Physics, Carleton University, Ottawa, Ontario K1S 5B6, Canada

[7]Centre for Research in Particle Physics, Carleton University, Ottawa, Ontario K1S 5B6, Canada

[8]CERN, European Organisation for Particle Physics, CH-1211 Geneva 23, Switzerland

[9]Enrico Fermi Institute and Department of Physics, University of Chicago, Chicago IL 60637, USA

[10]Fakultät für Physik, Albert Ludwigs Universität, D-79104 Freiburg, Germany

[11]Physikalisches Institut, Universität Heidelberg, D-69120 Heidelberg, Germany

[12]Indiana University, Department of Physics, Swain Hall West 117, Bloomington IN 47405, USA

[13]Queen Mary and Westfield College, University of London, London E1 4NS, UK

[14]Technische Hochschule Aachen, III Physikalisches Institut, Sommerfeldstrasse 26-28, D-52056 Aachen, Germany

[15]University College London, London WC1E 6BT, UK

[16]Department of Physics, Schuster Laboratory, The University, Manchester M13 9PL, UK

[17]Department of Physics, University of Maryland, College Park, MD 20742, USA

[18]Laboratoire de Physique Nucléaire, Université de Montréal, Montréal, Quebec H3C 3J7, Canada

[19]University of Oregon, Department of Physics, Eugene OR 97403, USA

[20]CLRC Rutherford Appleton Laboratory, Chilton, Didcot, Oxfordshire OX11 0QX, UK

[22]Department of Physics, Technion-Israel Institute of Technology, Haifa 32000, Israel

[23]Department of Physics and Astronomy, Tel Aviv University, Tel Aviv 69978, Israel

[24]International Centre for Elementary Particle Physics and Department of Physics, University of Tokyo, Tokyo 113-0033, and Kobe University, Kobe 657-8501, Japan

[25]Institute of Physical and Environmental Sciences, Brunel University, Uxbridge, Middlesex UB8 3PH, UK

[26]Particle Physics Department, Weizmann Institute of Science, Rehovot 76100, Israel

[27]Universität Hamburg/DESY, II Institut für Experimental Physik, Notkestrasse 85, D-22607 Hamburg, Germany

[28]University of Victoria, Department of Physics, P O Box 3055, Victoria BC V8W 3P6, Canada

[29]University of British Columbia, Department of Physics, Vancouver BC V6T 1Z1, Canada

[30]University of Alberta, Department of Physics, Edmonton AB T6G 2J1, Canada

[31]Duke University, Dept of Physics, Durham, NC 27708-0305, USA

[32]Research Institute for Particle and Nuclear Physics, H-1525 Budapest, P O Box 49, Hungary

[33]Institute of Nuclear Research, H-4001 Debrecen, P O Box 51, Hungary

[34]Ludwigs-Maximilians-Universität München, Sektion Physik, Am Coulombwall 1, D-85748 Garching, Germany

[a] and at TRIUMF, Vancouver, Canada V6T 2A3

[b] and Royal Society University Research Fellow

[c] and Institute of Nuclear Research, Debrecen, Hungary

[d] and Department of Experimental Physics, Lajos Kossuth University, Debrecen, Hungary

[e] on leave of absence from the University of Freiburg

1 Introduction

The lifetimes of b hadrons depend both on the strength of the b quark coupling to the lighter c and u quarks, and on the dynamics of b hadron decay. In the spectator model of heavy hadron decay, the decay of the heavy quark is unaffected by the presence of the other light quarks in the hadron, so the lifetimes of all hadrons containing the same heavy quark are predicted to be equal. This model fails badly for the charm hadrons, where the lifetime of the D^+ is more than 2.5 times the lifetime of the D^0 [1], but is a better approximation for the b hadrons, due to the larger mass of the b quark [2]. The difference between the B^+ and B^0 lifetimes[1] is expected to be at most 10 %, and depends on the details of the various non-spectator processes contributing to their decay. Measurements at the level of a few percent or better are therefore needed to test this prediction and probe the dynamics of b hadron decays.

Experimentally, most measurements of the B^+ and B^0 lifetimes have been performed using semileptonic decays, fully or partially reconstructing the decay products to distinguish B^+ from B^0 [3,4]. These measurements are limited due to the small branching ratios and limited reconstruction efficiencies for the selected final states. A more inclusive approach is to reconstruct resolvable secondary vertices from b hadron decays, since their long lifetimes lead to significant decay lengths [5,6]. In these analyses, the B^+ and B^0 decays are distinguished by reconstructing the charge of the secondary vertex. This technique results in much larger data samples, and offers the best hope of improving the precision. A measurement of this type is presented in the first part of this paper.

Inclusive samples of B^0 decays can also be used to search for CP and CPT violating effects. Although CP violation has so far been seen only in the neutral kaon system, possibly large effects are expected also in the B-meson system, so it is worthwhile to search for them even with the relatively small data samples collected at LEP. In the B^0-$\bar{B}^0$ system the weak eigenstates $|B^0\rangle$ and $|\bar{B}^0\rangle$ differ from the mass eigenstates $|B_1\rangle$ and $|B_2\rangle$:

$$
\begin{aligned}
|B_1\rangle &= \frac{(1 + \epsilon_B + \delta_B)|B^0\rangle + (1 - \epsilon_B - \delta_B)|\bar{B}^0\rangle}{\sqrt{2(1 + |\epsilon_B + \delta_B|^2)}} \\
|B_2\rangle &= \frac{(1 + \epsilon_B - \delta_B)|B^0\rangle - (1 - \epsilon_B + \delta_B)|\bar{B}^0\rangle}{\sqrt{2(1 + |\epsilon_B - \delta_B|^2)}}
\end{aligned}
\tag{1}
$$

where the parameters ϵ_B and δ_B parameterise indirect CP violation and CPT violation respectively [7]. These parameters can be studied using semi-leptonic b hadron decays, and limits of a few 10^{-2} have been set on both quantities [8–11]. A non-zero value of ϵ_B is also expected to produce time dependent asymmetries in inclusive B^0 *vs.* inclusive $\bar{B}^0$ decays [12]. This provides a second method to look for CP violating effects in b decays, and such an asymmetry is searched for in the second part of this paper. The same data sample is also used to test a basic prediction of CPT invariance, that the lifetimes of b and $\overline{b}$ hadrons are equal.

A brief overview of the analysis strategies is presented in Section 2, followed by a review of the data and Monte Carlo samples in Section 3. The parts common to both B^+ and B^0 lifetime and CP(T) violation analyses, namely the $b\overline{b}$ event tagging and b hadron production flavour tagging, are discussed in Sections 4 and 5. The lifetime analysis is described in detail in Section 6 and the CP and CPT violation analyses in Section 7. Finally, all the results and conclusions are summarised in Section 8.

2 Analysis Overview

The analyses exploit the characteristic topology of the $Z^0 \rightarrow b\overline{b}$ decay: two back-to-back jets aligned along the direction of the thrust axis. The event is divided into two hemispheres by the plane perpendicular to the thrust axis and containing the e^+e^- interaction point. One hemisphere (the 'tag

---

[1]Charge conjugate states are implied when discussing the lifetimes of individual b hadron species.

hemisphere' T) is tagged as containing a b decay using either a displaced secondary vertex or a high momentum lepton. The production flavour of the b hadron in the tag hemisphere (whether it originated from a b quark or $\overline{b}$ antiquark) is also determined, using jet, vertex and lepton charge information. The unbiased b decay in the other hemisphere (the 'measurement hemisphere' M) is used to perform the measurement of b hadron decay time.

The decay time of the b hadron in the measurement hemisphere is determined by reconstructing its decay vertex and energy. In the B^+ and B^0 lifetime analysis, this decay vertex is required to be significantly separated from the event primary vertex, and very strict requirements are placed on the confidence with which tracks are assigned to either this secondary vertex or the primary vertex. These requirements lead to a final data sample of only about 10 000 reconstructed vertices with well determined charge. The reconstructed decay times of the b hadrons giving rise to these charged and neutral vertices are then used to determine the lifetimes of the B^+ and B^0 mesons, employing the excess decay length technique [5, 13] to eliminate biases caused by the separated vertex requirement. The correlation of the sign of reconstructed charged b hadrons in the measurement hemisphere with the production flavour of the b hadron in the tag hemisphere is used to measure the probability of mis-reconstructing the b hadron charge.

In the CP(T) violation analysis, only the decay time of the b hadron in the measurement hemisphere is reconstructed. The charge is not determined, so no strict requirements are placed on the quality or separation of the b hadron vertex, leading to a much larger data sample of about 400 000 events. The production flavour of this b hadron is inferred from that of the b hadron in the tag hemisphere, aided by information in the measurement hemisphere, and taking into account the effects of B^0 and B_s mixing. The decay time distribution of decays tagged as b or $\overline{b}$ hadrons is then used to search for CP and CPT violating effects.

3 Data sample and event simulation

The OPAL detector is well described elsewhere [14–16]. The analyses described here rely mainly on charged particle track reconstruction using the central tracking chambers and the silicon microvertex detector. The b hadron lifetime analysis requires excellent pattern recognition, and uses only data taken between 1993 and 1995 with the upgraded silicon microvertex detector measuring tracks in both the r-ϕ and r-z planes [2] [16]. The CP(T) violation analysis also uses data taken in 1991 and 1992 with the original silicon microvertex detector measuring only in the r-ϕ plane [15].

Hadronic Z^0 decays were selected using standard criteria [17], additionally requiring at least 7 charged tracks in the event. The thrust axis polar angle $\cos\theta_T$ was calculated using charged tracks and electromagnetic clusters not associated to any track. To ensure the event was well contained within the acceptance of the detector, the thrust axis direction was required to satisfy $|\cos\theta_T| < 0.9$. The complete event selection has an efficiency of about 88 %, and selected a total of 2 390 221 events in the 1993–95 data and 754 372 events in the 1991-92 data.

Charged tracks and electromagnetic calorimeter clusters with no associated track were combined into jets using a cone algorithm [18], with a cone half angle of 0.65 rad and a minimum jet energy of 5 GeV. The transverse momentum p_t of each track was defined relative to the axis of the jet containing it, where the jet axis was calculated including the momentum of the track.

Monte Carlo simulated events were generated using JETSET 7.4 [19] with parameters tuned by OPAL [20]. The fragmentation functions of Peterson et al. [21] were used to describe the fragmentation of b and c quarks. The generated events were passed through a program that simulated the response of the OPAL detector [22] and through the same reconstruction algorithms as the data.

---

[2] A right handed coordinate system is used, with positive z along the e^- beam direction and x pointing towards the centre of the LEP ring. The polar and azimuthal angles are denoted by θ and ϕ, and the origin is taken to be the centre of the detector.

4 Tagging b$\overline{\text{b}}$ events

Two methods were used to tag b$\overline{\text{b}}$ events, based on displaced secondary vertices and high momentum leptons. The first method exploits the long lifetime, hard fragmentation, high decay multiplicity and high mass of b hadrons. An attempt was made to reconstruct a significantly separated secondary vertex in each jet of the event. If a secondary vertex was found, an artificial neural network was used to further separate b decays from charm and light quark background. The neural network has five inputs, derived from decay length, vertex multiplicity and invariant mass information. The algorithm is described fully in [23]. For this analysis, a hemisphere was defined to be tagged if any jet in the hemisphere had a secondary vertex with tag variable $B > 1.2$ [23], giving a hemisphere tagging efficiency of 32 % in b$\overline{\text{b}}$ events, and a non-b impurity of 12 %.

Electrons and muons with momentum $p > 2\,\text{GeV}$ and transverse momentum $p_t > 1\,\text{GeV}$ were also used to tag b$\overline{\text{b}}$ events[3]. Electrons were identified in the polar angle region $|\cos\theta| < 0.9$ using a re-optimised version of the neural network algorithm described in [24]. The identification relies on ionisation energy loss ($\mathrm{d}E/\mathrm{d}x$) measured in the tracking chamber, spatial and energy-momentum (E/p) matching between tracking and calorimetry, and the multiplicity measured in the presampler detectors. Photon conversions were rejected using another neural network algorithm [24]. Muons were identified in the polar angle region $|\cos\theta| < 0.9$ by requiring a spatial match between a track reconstructed in the tracking detectors and a track segment reconstructed in the external muon chambers, as in [25].

The tagged lepton hemispheres were further enhanced in semileptonic b decays by using information from the lepton p and p_t, and its degree of isolation from the rest of the jet, in a neural network algorithm [26]. This suppresses contributions from cascade (b $\rightarrow$ c $\rightarrow \ell$) decays (which have the wrong correlation of lepton sign with b hadron production flavour), charm and fake lepton background. The output S of the network was required to be greater than 0.7, giving a lepton sample about 75 % pure in b $\rightarrow \ell$ decays. The lepton tags contribute an additional 5 % to the hemisphere b-tagging efficiency, bringing the total to about 37 % with an impurity of 13 % in Monte Carlo.

The events used for the final analysis are those tagged by either of the b tagging methods described above (referred to as the T-tag) in one hemisphere, and passing the measurement selection requirements in the other hemisphere. These latter requirements are described below in Section 6.1 for the b hadron lifetime analysis and Section 7.1 for the CP(T) analysis, and are referred to as the M-tag. Both hemispheres are used as measurement hemispheres in events tagged by both tags in both hemispheres.

The b$\overline{\text{b}}$ purity of the combined tag T-M samples (tagged by the T-tag in one hemisphere and the M-tag in the other) were determined by applying an extension of the double tagging technique used for measuring R_b [23]. The number of hemispheres N_i tagged by tag i (i=T or M), and the number of events N_{ij} tagged by tag i in one hemisphere and tag j in the other hemisphere, are related to the total number N_had of events passing the event selection by:

$$
\begin{aligned}
N_i &= 2N_\text{had}\{\epsilon_i^\text{b}\,R_\text{b} + \epsilon_i^\text{c}\,R_\text{c} + \epsilon_i^\text{uds}\,(1 - R_\text{b} - R_\text{c})\}, \\
N_{ij} &= (2 - \delta_{ij})N_\text{had}\{C_{ij}^\text{b}\,\epsilon_i^\text{b}\epsilon_j^\text{b}\,R_\text{b} + C_{ij}^\text{c}\,\epsilon_i^\text{c}\epsilon_j^\text{c}\,R_\text{c} + C_{ij}^\text{uds}\,\epsilon_i^\text{uds}\epsilon_j^\text{uds}\,(1 - R_\text{b} - R_\text{c})\}.
\end{aligned}
\tag{2}
$$

Here ϵ_i^q gives the efficiency of tag i to tag hemispheres of flavour q (q=uds, c or b). The correlations C_{ij}^q are defined by $C_{ij}^\text{q} = \epsilon_{ij}^\text{q}/(\epsilon_i^\text{q}\epsilon_j^\text{q})$ where ϵ_{ij}^q is the efficiency to tag a q$\overline{\text{q}}$ event simultaneously with tag i in one hemisphere and tag j in the other. Deviations of C_{ij}^q from unity account for the fact that the tagging in the two hemispheres is not completely independent, there being small efficiency correlations for both physical and instrumental reasons. The quantities R_b and R_c are the fractions of hadronic Z^0 decays to b$\overline{\text{b}}$ and c$\overline{\text{c}}$, and were taken to be $R_\text{b} = 0.2170 \pm 0.0009$ and $R_\text{c} = 0.173 \pm 0.005$ [1].

The values of $\epsilon_\text{T}^\text{c}$ and $\epsilon_\text{T}^\text{uds}$ (which are known to be well modelled in Monte Carlo [23]) together with all the correlation terms C_{ij}^q, were determined from the Monte Carlo, and the values of N_had,

---

[3]The notation $c = 1$ is employed in this paper.

Data Sample	1993–95 b lifetime	1993–95 CP(T)	1991–92 CP(T)
Number of events	2 390 221	2 390 221	754 372
Number of T-M events	10 532	293 416	100 703
Combined tag purity (%)	94.8 ± 1.5	87.9 ± 2.6	81.8 ± 3.6
Statistical error	0.7	0.4	0.7
Systematic errors:			
T-tag uds efficiency	0.1	1.3	1.7
T-tag charm efficiency	0.3	0.4	0.7
Correlations (udsc events)	1.2	2.2	3.0
Correlations (b events)	0.5	0.4	0.4
R_c value	0.1	0.2	0.3
Total systematic error	1.3	2.6	3.5
Total error (%)	1.5	2.6	3.6

Table 1: The numbers of hadronic events, selected combined tag T-M events and tag purities for each of the data samples. The breakdown of statistical and systematic errors for each of the purity values is also given.

N_i and N_{ij} measured from the data. The five equations 2 were then solved using a χ^2 minimisation procedure to give the b-tagging efficiency $\epsilon_{\mathrm{T}}^{\mathrm{b}}$ of the T-tag, and all the tagging efficiencies $\epsilon_{\mathrm{M}}^{\mathrm{b}}$, $\epsilon_{\mathrm{M}}^{\mathrm{c}}$ and $\epsilon_{\mathrm{M}}^{\mathrm{uds}}$ of the M-tag. The b-purity Π_{TM} of the combined tag T-M sample was then calculated as:

$$\Pi_{\mathrm{TM}} = \frac{C_{\mathrm{TM}}^{\mathrm{b}} \ \epsilon_{\mathrm{T}}^{\mathrm{b}}\epsilon_{\mathrm{M}}^{\mathrm{b}} \ R_{\mathrm{b}}}{C_{\mathrm{TM}}^{\mathrm{b}} \ \epsilon_{\mathrm{T}}^{\mathrm{b}}\epsilon_{\mathrm{M}}^{\mathrm{b}} \ R_{\mathrm{b}} + C_{\mathrm{TM}}^{\mathrm{c}} \ \epsilon_{\mathrm{T}}^{\mathrm{c}}\epsilon_{\mathrm{M}}^{\mathrm{c}} \ R_{\mathrm{c}} + C_{\mathrm{TM}}^{\mathrm{uds}} \ \epsilon_{\mathrm{T}}^{\mathrm{uds}}\epsilon_{\mathrm{M}}^{\mathrm{uds}} \ (1 - R_{\mathrm{b}} - R_{\mathrm{c}})}. \qquad (3)$$

The results of this procedure are given in Table 1 for the three data samples: 1993–95 data with the M-tag used to measure the b hadron lifetime, and 1993–95 and 1991-92 data with the M-tag used in the CP(T) analysis. In the last case, the T-tag used vertexing in the r-ϕ plane only [23], and the purity is correspondingly lower. The purity is somewhat higher for the b lifetime analysis, as the requirements on the M-tag secondary vertex also provide some rejection of non-b background. In contrast, the CP(T) M-tag has almost equal efficiency for all flavours.

The systematic errors resulting from each of the inputs used in the fits for the b purity are also given in Table 1. They were evaluated using the methods and parameter ranges discussed in [23]. The efficiency errors include the effects of charm and light quark physics uncertainties, tracking resolution and lepton identification. The hemisphere tagging correlations for $b\overline{b}$ events are slightly larger than those in [23], and a systematic uncertainty of ± 0.02 on the C_{ij}^{b} values is estimated, in addition to the Monte Carlo statistical errors. The correlations are larger because of stronger geometrical effects at large values of $|\cos\theta_T|$. The uncertainties on the uds and $c\overline{c}$ correlations C_{ij}^{uds} and C_{ij}^{c} include systematic errors of ± 0.2 but are still dominated by Monte Carlo statistics. The error from uncertainty in the value of R_{b} is negligible.

5 Tagging the b production flavour

The production flavour (b or $\overline{\mathrm{b}}$) of the b hadron in the T-tagged hemisphere was determined using up to three pieces of information in each event: the momentum-weighted average track charge, or 'jet charge'; the charge of a secondary vertex reconstructed in the hemisphere; and the charge of a high momentum lepton in the hemisphere. The jet charge can be calculated for every tagged hemisphere, and either or both of the vertex or lepton charges is always available as a consequence of the b-tagging techniques used. The three charges were combined using a neural network algorithm to produce a single production flavour tag variable Q_{T} for each T-tagged hemisphere.

6

The jet charge $Q_{\rm jet}$ was calculated for the highest energy jet in the T-tag hemisphere as:

$$Q_{\rm jet} = \frac{\sum_i (p_i^l)^\kappa q_i}{\sum_i (p_i^l)^\kappa} \tag{4}$$

where p_i^l is the longitudinal momentum component with respect to the jet axis and q_i the charge (± 1) of track i, and the sum was taken over all the tracks in the jet. The parameter κ was set to 0.5 to optimise the separation between hemispheres containing b and $\bar{\rm b}$ hadrons, including the effects of B^0 and $B_{\rm s}$ mixing [27].

For hemispheres tagged by a secondary vertex, the charge of this vertex $Q_{\rm vtx}$ was calculated as:

$$Q_{\rm vtx} = \sum_i w_i q_i \tag{5}$$

and the uncertainty $\sigma_{Q_{\rm vtx}}$ as:

$$\sigma_{Q_{\rm vtx}}^2 = \sum_i w_i (1 - w_i) q_i^2 \tag{6}$$

where w_i is the weight for track i to have come from the secondary, rather than the primary, vertex [28]. The weights w_i were obtained from a neural network algorithm using as input the track momentum, transverse momentum with respect to the jet axis, and impact parameters with respect to the reconstructed primary and secondary vertices, as in [27]. A well reconstructed vertex charge (with small $\sigma_{Q_{\rm vtx}}$) close to $+1$ (-1) indicates a B^+ (B^-), tagging the hemisphere as containing a $\bar{\rm b}$ (b) quark, whilst a vertex charge close to zero indicates a neutral b hadron (e.g. B^0 or $\bar{B}^0$), giving no information on the production flavour. A vertex charge with large $\sigma_{Q_{\rm vtx}}$ cannot distinguish between $Q_{\rm vtx} = 0$ or $Q_{\rm vtx} = \pm 1$, so again provides no information on the production flavour.

For hemispheres tagged by a lepton, the lepton charge gives an estimate of the b production flavour, diluted by B^0 and $B_{\rm s}$ mixing, cascade b decays, charm decays and fake leptons. The product $Q_\ell S$ of the lepton charge Q_ℓ and the output S of the neural network used to select $b \to \ell$ decays (see Section 4) was used as a tagging variable analogous to $Q_{\rm jet}$ and $Q_{\rm vtx}$. Higher values of S indicate greater probability of the lepton originating from a semileptonic b decay.

The available production flavour estimates for each T-tagged hemisphere were combined into a single estimate $Q_{\rm T}$ using a neural network algorithm, as in [27]. The neural network has four inputs: the jet charge $Q_{\rm jet}$, the vertex charge $Q_{\rm vtx}$ and its error $\sigma_{Q_{\rm vtx}}$, and the lepton tag $Q_\ell S$. Separate neural networks with fewer inputs were trained for use in hemispheres with only a vertex or a lepton. The variable $Q_{\rm T}$ is defined such that:

$$Q_{\rm T} = \frac{N_{\rm b}(x) - N_{\bar{\rm b}}(x)}{N_{\rm b}(x) + N_{\bar{\rm b}}(x)}$$

where $N_{\rm b}(x)$ and $N_{\bar{\rm b}}(x)$ are the numbers of Monte Carlo b hadron and $\bar{\rm b}$ hadron hemispheres with a particular value of the neural network output x. Thus hemispheres with $Q_{\rm T} = +1$ are tagged with complete confidence as b hadrons, hemispheres with $Q_{\rm T} = -1$ with complete confidence as $\bar{\rm b}$ hadrons, and hemispheres with $Q_{\rm T} = 0$ are equally likely to be b or $\bar{\rm b}$ hadrons. The modulus $|Q_{\rm T}|$ satisfies $|Q_{\rm T}| = 1 - 2\eta$, where η is the 'mis-tag probability', i.e. the probability to tag the production flavour incorrectly.

For the CP(T) violation analysis, both the production flavour estimate from the T-tag hemisphere and the jet charge $Q_{\rm jet}$ in the M-tag hemisphere are used to infer the production flavour of the b hadron in the M-tag hemisphere. In this hemisphere, the parameter κ in equation 4 is set to zero, so the jet charge becomes simply the average of the charges of the tracks in the jet. This avoids being sensitive to the decay flavour of mixed or unmixed B^0 and $B_{\rm s}$ mesons, but is still sensitive to the production flavour of the b hadron via the information carried by the fragmentation tracks in the

jet [29]. This jet charge is used to produce a tagging variable Q_M defined similarly to Q_T for the T-tag hemisphere. The information from both hemispheres is combined into a single variable Q_2, defined as:

$$Q_2 = 2\left\{\frac{(1-Q_T)(1+Q_M)}{(1-Q_T)(1+Q_M) + (1+Q_T)(1-Q_M)}\right\} - 1$$

The variable Q_2 is positive (negative) if the event is tagged as containing a b ($\overline{\text{b}}$) hadron in the M-tag hemisphere.

The Q_{jet} and Q_{vtx} distributions are not charge symmetric because of detector effects causing a difference in the rate and reconstruction of positive and negative tracks. These effects are caused by the detector material and the Lorentz angle in the tracking chambers [10]. They were removed by subtracting offsets from the Q_{jet} and Q_{vtx} values before the calculation of Q_T and Q_M. The offsets were determined from data using the inclusive T-tagged samples, and were found to be fractions 0.018 ± 0.002, 0.034 ± 0.002 and 0.028 ± 0.002 of the RMS width of the $Q_{jet}(\kappa = 0.5)$, $Q_{jet}(\kappa = 0)$ and Q_{vtx} distributions, respectively.

The distributions of Q_T and Q_M in T-tagged data and Monte Carlo events are shown in Figures 1(a) and 1(b). The sharp drop at about $|Q_T| = 0.8$ in Figure 1(a) is due to the irreducible fraction of lepton tagged events that are tagged incorrectly due to B^0 and B_s mixing. Around 30 % of events have equal numbers of positive and negative tracks in the jet in the M-tag hemisphere, giving zero jet charge and $Q_M = 0$. These events are not shown in Figure 1(b). Some discrepancies between data and Monte Carlo distributions are visible. These discrepancies are not important, provided that the Q_T values in data correctly describe the data mistag probabilities. To check that this is the case, events where both hemispheres are T-tagged, yielding b production flavour estimates Q_{T1} and Q_{T2}, were used. Since the two hemispheres must contain b hadrons produced with opposite flavour, the product $\xi_{TT} = Q_{T1}Q_{T2}$ is negative if both (or neither) hemispheres are tagged correctly, and positive if only one is tagged incorrectly. The distribution $f(\xi_{TT})$ of ξ_{TT} in data thus allows the production flavour estimate Q_T to be checked. The function:

$$g(\xi_{TT}) \equiv \frac{f(\xi_{TT})}{f(\xi_{TT}) + f(-\xi_{TT})} \quad \{\text{for } \xi_{TT} > 0\} \tag{7}$$

represents the 'wrong sign fraction' at a particular value of $|\xi_{TT}|$, and should satisfy $g(\xi_{TT}) = (1 - \xi_{TT})/2$ if Q_T correctly describes the mis-tag probabilities. The distribution $g(\xi_{TT})$ in data is shown in Figure 1(c), together with a linear fit. The distribution has the expected form, and the fitted gradient is $dg/d\xi_{TT} = -0.514 \pm 0.012$, showing that the average magnitude of Q_T is correct to a relative precision of 2.6 %.

The same technique was used to study Q_M, via the 'cross-tag' product $\xi_{TM} = Q_{T1}Q_{M2}$, as Q_M has a smaller tagging power than Q_T. The function $g(\xi_{TM})$ was defined in an analogous way to $g(\xi_{TT})$ in equation 7. The distribution $g(\xi_{TM})$ in data is shown in Figure 1(d), and the corresponding gradient is -0.545 ± 0.018. Since Q_T has already been shown above to be correct to 2.6 %, all of this discrepancy is attributed to Q_M, which therefore has a bias of up to about 10 %. These values are used to calculate tagging systematic errors.

6   B$^+$ and B^0 lifetime analysis

The b$\overline{\text{b}}$ event tagging and production flavour tagging described above is common to both the b hadron lifetime and CP(T) analyses. The remainder of each analysis—the M-tag and the fits to the data—are specific to each analysis. The b hadron lifetime analysis is described in this section, and the CP(T) analysis in Section 7.
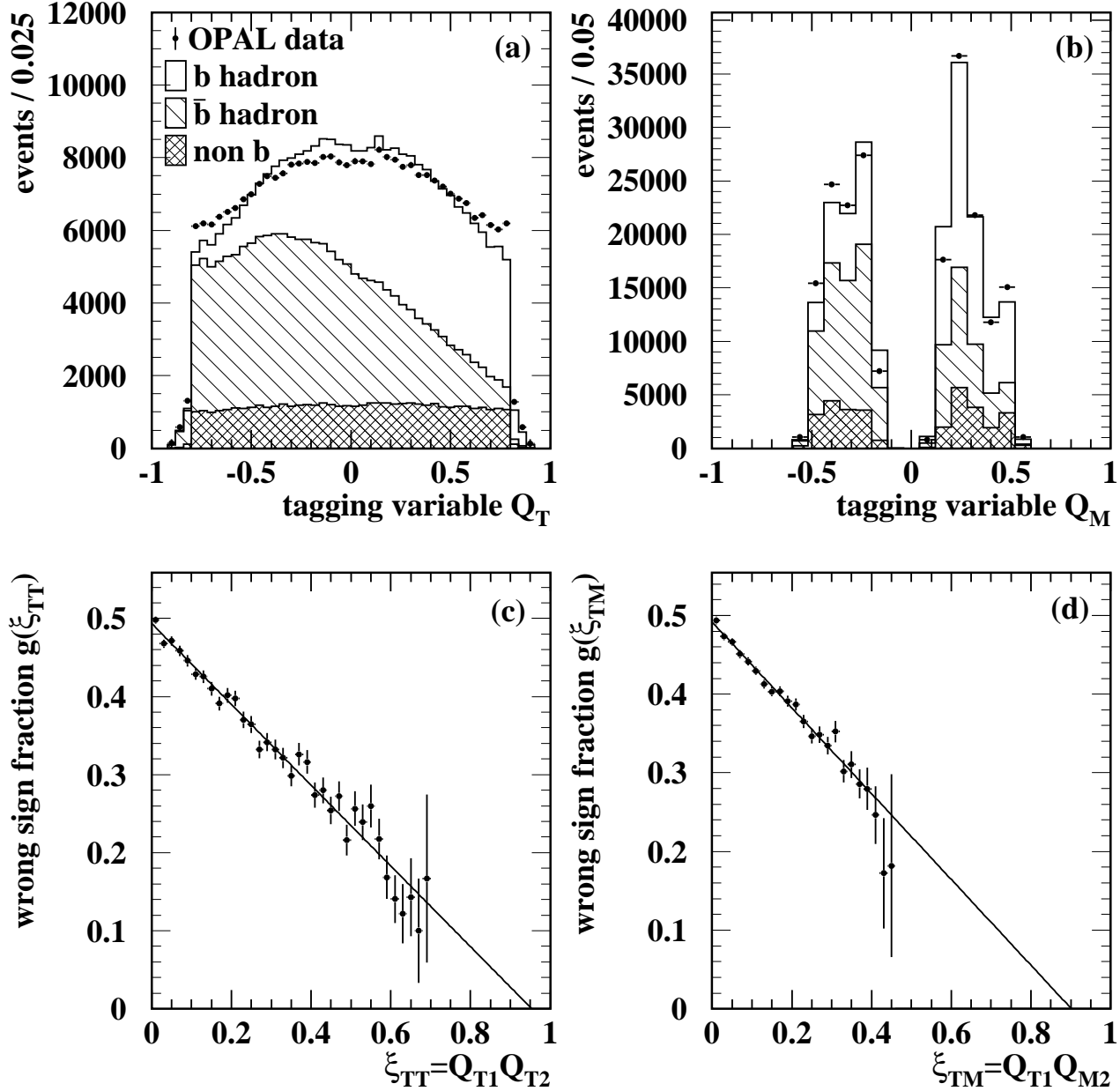
Figure 1: Production flavour tagging of $b\overline{b}$ events: (a) Distribution of the flavour tagging variable Q_T in data (points) and Monte Carlo (histogram) T-tagged hemispheres. The contributions from b hadrons, $\overline{b}$ hadrons and non-b backgrounds are shown. (b) The analogous distributions for the M-tag hemispheres. The 30 % of the sample (90000 events in data) with $Q_M = 0$ are not shown. In both (a) and (b), the error bars on the data points are smaller than the symbols. (c) Distribution of the wrong sign fraction $g(\xi_{TT})$ in data double T-tagged events, with a linear fit superimposed. (d) Distribution of the wrong sign fraction $g(\xi_{TM})$ in data double T-tagged events, again with a linear fit superimposed.

6.1   b hadron reconstruction

The b hadron reconstruction used for the M-tag in this analysis is similar to that used in [5]. It aims to reconstruct a relatively small sample of clear secondary vertices where each track can be unambiguously associated to either the primary or secondary vertex.

The algorithm considers all tracks in a jet which have momentum $p > 0.5\,\text{GeV}$, impact parameter (in the r-ϕ plane) $|d_0| < 1\,\text{cm}$ and error on the impact parameter $\sigma_{d_0} < 0.1\,\text{cm}$. All possible sets of assignments of these tracks to the primary and secondary vertices ('arrangements') were considered, requiring at least two tracks to be assigned to the secondary vertex, and including the combination where no tracks at all are assigned to the primary vertex.

The positions of the two vertices in each arrangement were determined by fitting all the assigned tracks to a common vertex in three dimensions. For the primary vertex, an additional constraint from the average beam spot position was used, determined from a fit to the tracks in many consecutive events [30]. The χ^2 of the arrangement was calculated as the sum of the χ^2 values for the primary and secondary vertex fits, and the fit probability of the arrangement determined from the χ^2 value and the number of degrees of freedom in the two vertex fits.

For the jet to be accepted as having a clear secondary vertex, the following conditions had to be satisfied:

1. One and only one arrangement (the 'best arrangement') has a fit probability exceeding 1 %.

2. All other arrangements have a χ^2 value exceeding that of the best arrangement by at least 4.

3. The decay length L of the secondary vertex, divided by its error σ_L, satisfies $L/\sigma_L > 3$. The decay length is calculated from the distance between the fitted primary and secondary vertices, using the direction of the jet axis as a constraint [23].

4. The decay length must be positive, but less than 3 cm. The decay length is positive if the secondary vertex is displaced from the primary vertex in the same direction as the jet momentum vector.

These requirements ensure that the best arrangement has an acceptable probability, that no other arrangement is likely to be the correct one, and that the primary and secondary vertices are well separated. Jets containing b hadrons with short decay lengths will tend to fail requirements 2 or 3, whilst those with a mis-measured track which does not fit with either the primary or secondary vertex will tend to fail requirement 1.

The charge Q of the secondary vertex and its error σ_Q were then calculated, using equations 5 and 6, with track weights w_i optimised for this vertex finding algorithm. To ensure the vertex charge was well reconstructed, the error σ_Q was required to be less than 0.7. All tracks in the jet were used in calculating the vertex charge, including those which failed the tighter selection used for the initial vertex finding.

A total of 10 532 combined T-M tagged events were found in the data with this selection for the M-tag. The distribution of the M-tag vertex charge, together with the Monte Carlo prediction, is shown in Figure 2. Clear peaks at $Q = \pm 1$ and 0 are seen, corresponding to high purities of charged and neutral b hadrons. In the Monte Carlo, the neutral b hadrons are a mixture of approximately 63 % B^0, 24 % B_s and 13 % b baryons (denoted by Λ_b). The charged b sample is almost entirely B^+, with a very small contribution from charged b baryons (Ξ_b^-) which is estimated at about 1 % and is neglected.

6.2   Excess proper time reconstruction

The decay length distributions of secondary vertices selected by the above algorithm in data and Monte Carlo are shown in Figure 3(a). The decay lengths are very biased towards large values, since
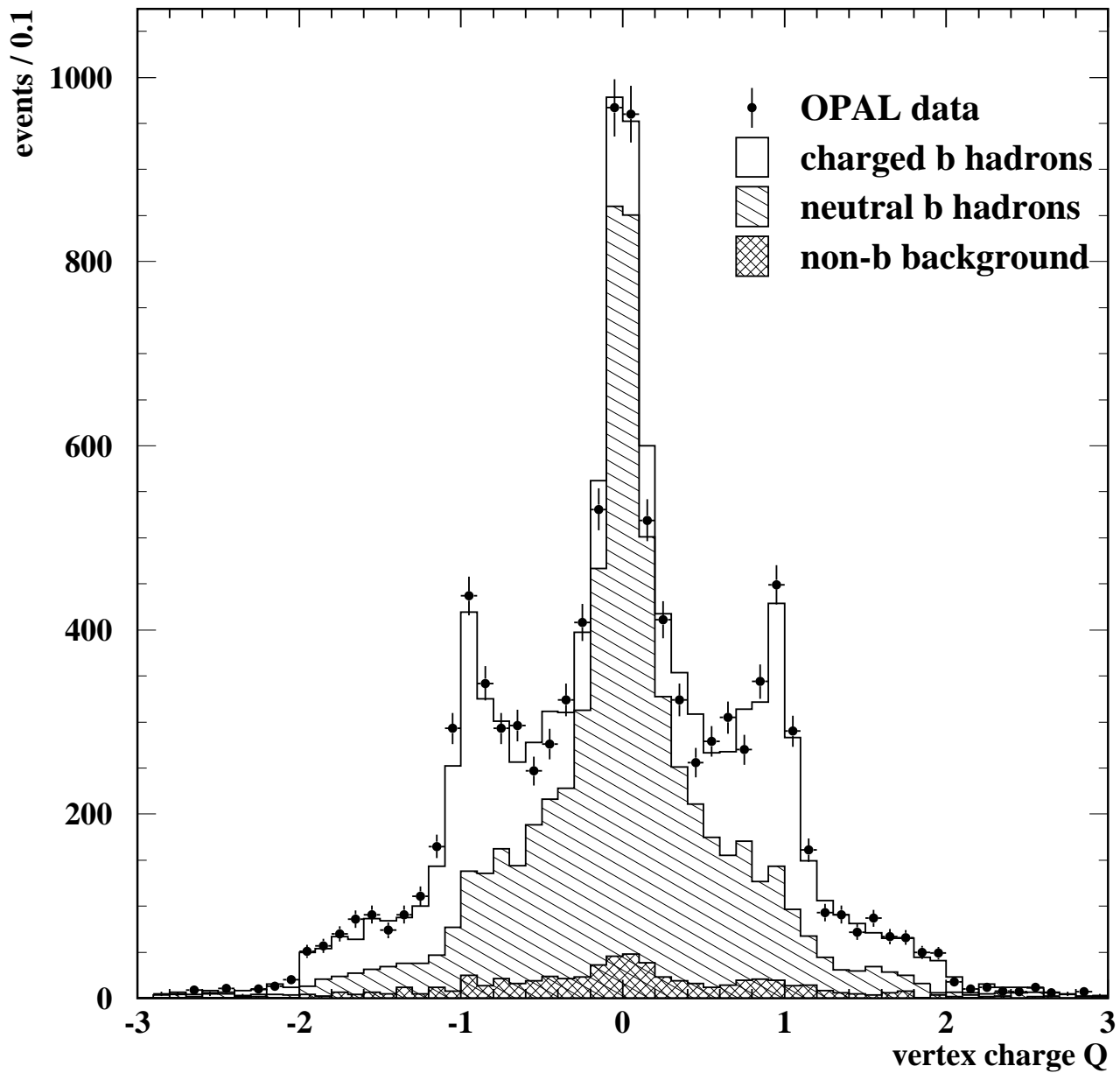
Figure 2: Distributions of the vertex charge Q in the data (points) and Monte Carlo (histogram), normalised to the same number of entries. The expected contributions from charged b hadrons, neutral b hadrons and non-b background are indicated.

the algorithm preferentially selects well separated secondary vertices. Therefore in order to extract the b hadron lifetimes, the excess decay length method is used, as in [5,13]. For each selected event, the minimum b hadron decay length that would still result in a resolvable secondary vertex passing all the requirements described in Section 6.1 was determined. To find this minimum decay length, all the tracks assigned to the secondary vertex in the best arrangement were assumed to come from the b hadron. They were then translated along the direction of the jet axis towards the primary vertex (as if the b hadron had decayed at an earlier time), and the entire vertex selection repeated (requirements 1–4 of Section 6.1 and $\sigma_Q < 0.7$, including recalculating the χ^2 values for all possible vertex arrangements). The translation distance at the point where the modified arrangement just fails one of the requirements defines the excess decay length L_{ex}. The distributions of L_{ex} in data and Monte Carlo are shown in Figure 3(b).

For most selected vertices, the point of failure occurs when one of the less good arrangements has an improved χ^2, and fails requirements 1 or 2. Others fail because the L/σ separation becomes too small or the vertex charge error σ_Q becomes too large.

The distribution of excess decay length is approximately a negative exponential, with the same slope as the b hadron decay length distribution before the vertex selection requirements were imposed. The distribution is exactly an exponential provided that the assignment of b hadron decay tracks to the secondary vertex and fragmentation tracks to the primary vertex is correct, and that the effects of vertex resolution and the lifetime of the charm hadron produced in the b hadron decay can be neglected.

That the distribution is exponential is most easily seen in terms of the excess decay proper time, obtained from the excess decay length via the reconstruction of the b hadron energy. The effect of the charm hadron lifetime will be considered first. Ignoring resolution effects, the rate of events $F(t)$ with excess decay time t is given by the convolution of the lifetime exponentials e^{-t_b/τ_b} and e^{-t_c/τ_c} for the decaying b and charm hadrons. Here t_b is the decay time and τ_b the lifetime of the b hadron, and similarly for the charm hadron. The convolution is obtained by integrating over the excess decay time t' of the b hadron, defined as $t' = t_b - t_0$, where t_0 is the minimum decay time for this event to pass the vertex selection requirements. Since the introduction of excess decay time just corresponds to the redefinition of zero time at $t_b = t_0$ and does not affect the form of the b lifetime exponential, the distribution $F(t)$ is given by replacing t_b by t', t_c with $t - t'$, and integrating:

$$
\begin{aligned}
F(t) \quad &\propto \quad \int_a^b e^{-t'/\tau_b} e^{-(t-t')/\tau_c} \, dt' \\
&\propto \quad e^{-t/\tau_c} \left[e^{-t'(1/\tau_b - 1/\tau_c)} \right]_{t'=a}^{t'=b}
\end{aligned}
$$

where normalisation factors have been neglected. The upper limit b is simply given by $b = t$, as only b hadrons decaying with excess time smaller than t can contribute. The lower limit $a = -t_0$, corresponding to b hadrons decaying at $t_b = 0$. As long as this minimum b hadron excess decay time is in magnitude much larger than the maximum contributing charm decay time, the lower limit can be approximated by $a = -\infty$. The requirements of Section 6.1 select events with a single secondary vertex well separated from the primary vertex. This ensures a long b hadron decay time, and suppresses events with a resolvable tertiary vertex from a long-lived charm hadron, effectively truncating the charm decay exponential. These conditions ensure that the approximation $a = -\infty$ is valid, and the integral finally becomes

$$
F(t) \propto e^{-t/\tau_b} \ .
$$

A similar argument holds for the effect of the finite detector resolution. In this case, the resolution function replaces the charm hadron lifetime exponential in the convolution, and the limits become $a = -\infty$ and $b = \infty$. Since the convolution of an exponential with any finite function is another exponential with the same decay constant as the original, the b hadron lifetime distribution is again recovered.
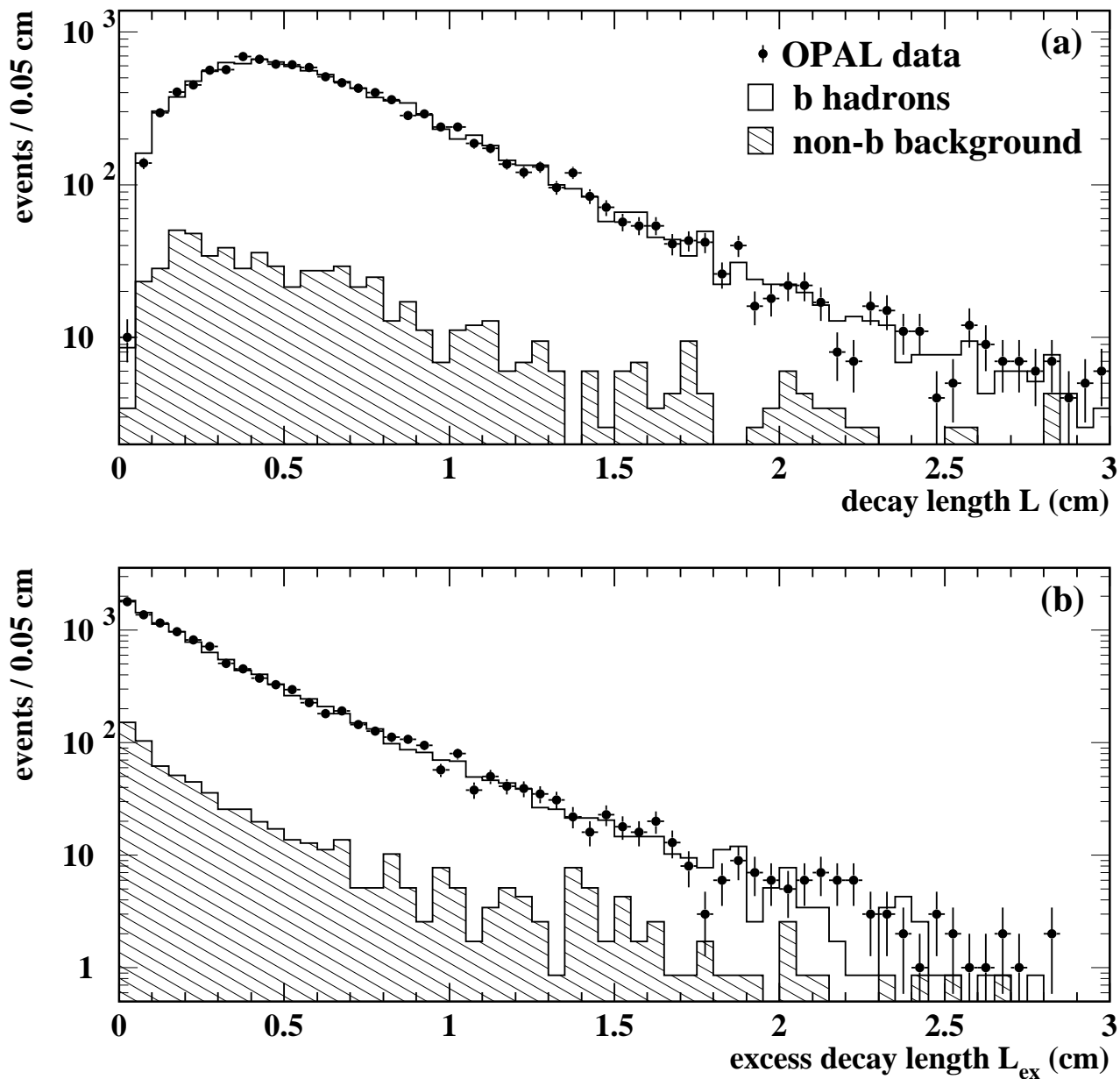
Figure 3: Distributions of (a) decay length L and (b) excess decay length L_{ex} in data (points with error bars) and Monte Carlo (histogram), for all selected secondary vertices. The expected contributions of b hadrons and non-b background are indicated.

However, for a small fraction of events (mainly those with low L_{ex}), one or more tracks are misassigned from the primary to the secondary vertex or *vice versa*, which introduces distortions in the excess decay length and proper time distributions. Such events also tend to have some tracks with vertex charge weights $w_i \approx 0.5$ (*i.e.* not clearly assigned to either vertex), and so are concentrated in the regions of Q away from the peaks at integer values.

The excess decay length was combined with an estimate of the b hadron energy E_b in each event to determine the excess proper time t, via the relation:

$$t = \frac{m_b L_{ex}}{\sqrt{E_b^2 - m_b^2}}$$

where m_b is the b hadron mass, taken to be that of the B^+ and B^0, *i.e.* 5.279 GeV [1]. The b hadron energy was estimated using a technique described in [31]. First, the energy of the b jet E_{bjet} was estimated by treating the event as a two-body decay of a Z^0 into a b jet of mass m_b and another object making up the rest of the event. Then, the charged and neutral fragmentation energy E_{bfrag} in the b jet was estimated using the charged track weights w_i, and the unassociated electromagnetic calorimeter clusters weighted according to their angle with respect to the jet axis. Finally the b hadron energy was calculated as $E_b = E_{bjet} - E_{bfrag}$.

The resulting distributions of b hadron energy in data and Monte Carlo are shown in Figure 4(a). The agreement is generally good, and the small differences around the peak are within the uncertainties due to the imprecise knowledge of b fragmentation. In addition to all the vertex requirements described above, selected M-tag hemispheres were required to have $E_b > 20$ GeV, which suppresses to a negligible level events where the M-tagged jet originates from a gluon and not a b quark. This cut is included in the definition of the M-tag and is included in the event counts and purities of Table 1. The energy resolution in Monte Carlo $b\bar{b}$ events is shown in Figure 4(b). The reconstructed energy has a mean equal to the true energy, but has asymmetric tails. However, these tails are small enough not to have a significant effect on this analysis.

6.3 Fit and results

The lifetimes of the B^+ and B^0 mesons were extracted by using a maximum likelihood fit to the mean excess proper time t as a function of the modulus of the vertex charge Q. All events with $0 < t < 15$ ps were used in the fit. The data were divided into ten bins between $|Q| = 0$ and $|Q| = 2$, and all events with $|Q| > 2$ put into an eleventh bin. The mean excess decay time $\langle t \rangle_j$ was then calculated for each $|Q|$ bin j, and compared to the fit prediction τ_j. The latter depends on the lifetime τ_s of each source s (b hadron type or background) and the fraction of each source f_s^j expected in bin j.

The fractions f_s^j depend on the vertex charge Q. If the charge tagging were perfect, only charged b hadrons would be expected at $Q = \pm 1$, and only neutral b hadrons at $Q = 0$. However, there is some cross-contamination, as can be seen in Figure 2. As the measurement of the B^+ and B^0 lifetimes depends crucially on the level of this contamination, this was fitted from the data by exploiting the correlation of the vertex charge Q with the opposite (T-tag) hemisphere b production flavour estimate Q_T. For example, a b hadron in the T-tag hemisphere implies a $\bar{b}$ hadron[4] (B^-, $\bar{B}^0$, $\bar{B}_s$ or Λ_b) in the M-tag hemisphere, giving a correctly reconstructed charge of $Q = -1$ or $Q = 0$. The number of such events reconstructed with $Q = +1$ therefore gives information on the number of neutral b hadrons incorrectly reconstructed as charged b hadrons, since a true B^+ (being a b rather than a $\bar{b}$ hadron) cannot be opposite another b hadron. In fact, the charged/neutral separation is a function of the continuous variable Q, and is described by a parameterisation constrained by the above correlation. These parameters were determined at the same time as the source lifetimes τ_s as additional parameters in the fit.

---

[4]By convention, the b mesons considered as particles (B^+, B^0, B_s) contain a $\bar{b}$ antiquark, and the antiparticles (B^-, $\bar{B}^0$, $\bar{B}_s$) contain a b quark. The opposite is true for baryons, so a Λ_b contains a b quark and a $\bar{\Lambda}_b$ contains a $\bar{b}$ antiquark.
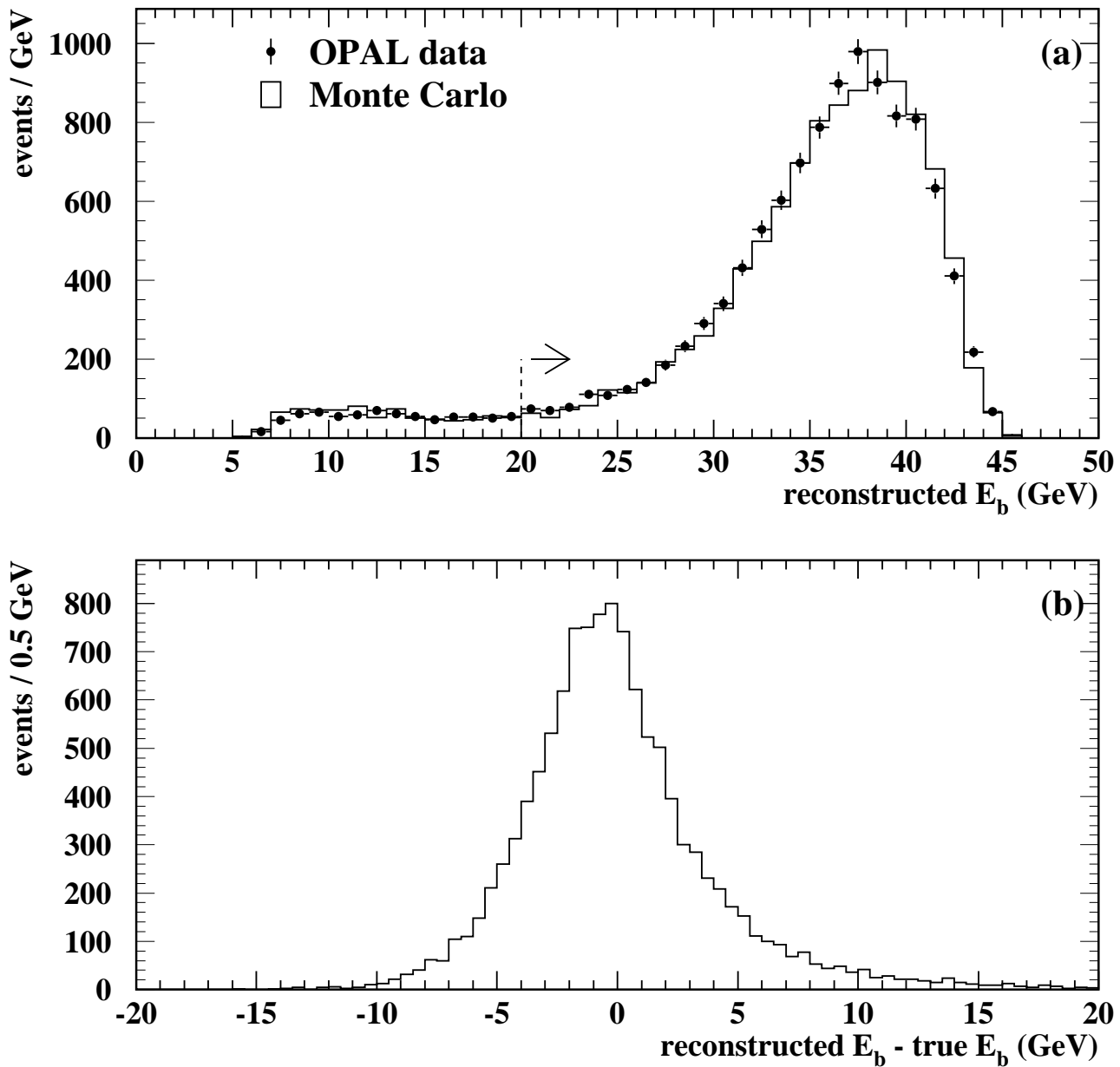
Figure 4: (a) Reconstructed b hadron energy distributions for data (points with error bars) and Monte Carlo (histogram). The position of the minimum energy cut is shown by the arrow. (b) Resolution of the reconstructed b hadron energy in Monte Carlo b$\overline{\text{b}}$ events, after the minimum energy cut has been applied.

In more detail, the total likelihood of the event sample was given by:

$$\mathcal{L} = \mathcal{L}^{\text{time}} \cdot \prod_i \mathcal{L}_i^{\text{tag}} \tag{8}$$

where $\mathcal{L}^{\text{time}}$ represents the likelihood from the fit to the lifetime as a function of vertex charge Q and $\mathcal{L}_i^{\text{tag}}$ represents the likelihood of each event used to determine the charged/neutral separation. The former is calculated in bins of Q, whilst the latter is determined event by event, and the product is taken over all events i.

The logarithm of the time likelihood $\mathcal{L}^{\text{time}}$ is given by:

$$\ln \mathcal{L}^{\text{time}} = \sum_j -N_j \left(\frac{\langle t \rangle_j}{\tau_j} + \ln \tau_j \right)$$

where the index j runs over the bins of vertex charge Q. The term inside the sum represents the log-likelihood to measure a mean decay time $\langle t \rangle_j$ in a sample of N_j events distributed according to a negative exponential with lifetime τ_j. Although the data events are not distributed according to a single exponential, the differences are sufficiently small that this expression can be used. The expected true mean decay time in bin j is given by:

$$\tau_j = D(\langle Q \rangle_j) + \sum_s f_s^j \tau_s \tag{9}$$

where f_s^j is the fraction of events from source s in bin j, and τ_s is the lifetime of source s. There are nine sources in total:

$$s = \{\text{B}^+, \text{B}^-, \text{B}^0, \bar{\text{B}}^0, \text{B}_s, \bar{\text{B}}_s, \bar{\Lambda}_b, \Lambda_b, \text{background}\}$$

and the lifetimes of particle and antiparticle are assumed to be equal ($\tau_{\text{B}+} = \tau_{\text{B}-}$ etc). The background is characterised by a lifetime τ_{bg}, taken from Monte Carlo.

The function $D(\langle Q \rangle_j)$ in equation 9 accounts for the distortions in the excess decay length distribution caused by mis-assigned tracks discussed in Section 6.2. These can be seen in Figure 5, which shows the mean excess proper time $\langle t \rangle$ as a function of $|Q|$ for both data (points) and Monte Carlo (solid line). Events which have one or more mis-assigned tracks tend to have smaller than average excess proper time, and to be concentrated away from integer values of Q. This reduces the mean excess decay time in these regions, and consequently increases the mean time close to integer values of Q. This effect, seen clearly in both data and Monte Carlo, is parameterised by the periodic correction function D, which has the form:

$$D(q) = d(q - 1/2)^2 - d/8 \quad \{\text{for } 0 < q < 1\} \tag{10}$$

where $q = (Q - \text{int}(Q))$ is the non-integer part of Q. The parameter d characterises the amplitude of the distortion, and is left as a free parameter in the fit. The functional form of this correction was chosen by studying the effect in Monte Carlo.

The second part of the overall likelihood in equation 8 is the tag likelihood $\mathcal{L}^{\text{tag}}$. It is given for each event i by:

$$\mathcal{L}_i^{\text{tag}} = \sum_s P_s^Q(Q_i) P_s^T(Q_{\text{T}i}) \tag{11}$$

The function $P_s^Q(Q)$ gives the probability of each source s as a function of the b hadron vertex charge Q. For the B$^+$ this function is given by:

$$P_{\text{B}+}^Q(Q) = \begin{cases} (1 - f_{\text{bg}})c_3 & \text{for } Q \leq -1 \\ (1 - f_{\text{bg}})(c_0 + (c_0 - c_3)Q) & \text{for } -1 < Q \leq 0 \\ (1 - f_{\text{bg}})(c_0 + (c_1 - c_0 - c_2)Q + c_2 Q^2) & \text{for } 0 < Q < 1 \\ (1 - f_{\text{bg}})c_1 & \text{for } Q \geq 1 \end{cases}$$
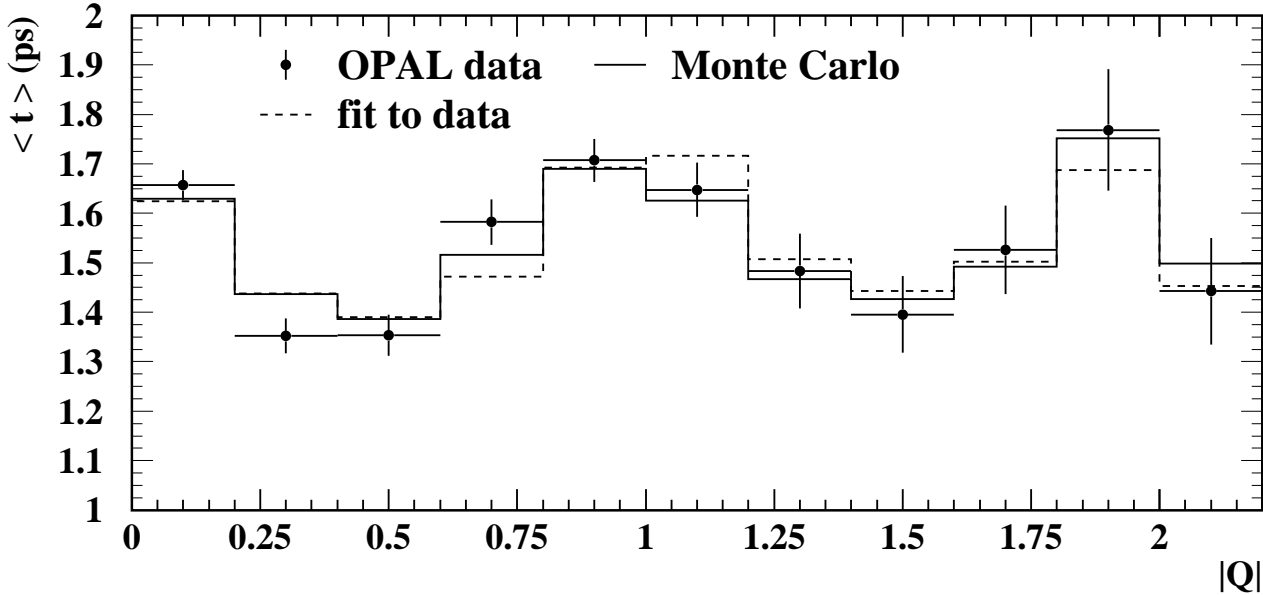
Figure 5: The distribution of mean excess decay time $\langle t \rangle$ as a function of the modulus of the vertex charge $|Q|$. The data are shown by the points with error bars, and the Monte Carlo (reweighted to the same B^+ and B^0 lifetimes as measured in the data) distribution is shown by the solid line. The prediction of the fit is shown by the dashed line. The bin between $|Q| = 2$ and $|Q| = 2.2$ contains all events with $|Q| > 2$.

where f_{bg} is the fraction of non-$b\bar{b}$ background, c_0 represents the fraction of signal B^+ events at $Q = 0$, and c_1 the fraction of signal B^+ events at $Q = 1$. A quadratic interpolation with coefficient c_2 is used in the range $0 < Q < 1$, and the fraction of B^+ is constant for $Q \geq 1$. A small fraction c_3 of B^+ events has $Q \leq -1$, and a linear interpolation is used for the fraction of B^+ between -1 and 0. This functional form is illustrated in Figure 6 and is seen to give a reasonable description of the B^+ fraction in Monte Carlo. Large variations in the parameters c_0 and c_3 are considered when assessing the systematic errors.

The fraction of B^- is given by charge symmetry: $P_{\mathrm{B}^-}^Q(Q) = P_{\mathrm{B}^+}^Q(-Q)$. The remaining signal fraction is neutral b hadrons, so the fractions of B^0 and $\bar{B}^0$ are given by:

$$P_{\mathrm{B}^0}^Q(Q) = P_{\bar{\mathrm{B}}^0}^Q(Q) = (1 - f_{\mathrm{B_s}}^0 - f_{\Lambda_b}^0)(1 - f_{\mathrm{bg}} - P_{\mathrm{B}^+}^Q(Q) - P_{\mathrm{B}^-}^Q(Q)) \qquad (12)$$

where $f_{\mathrm{B_s}}^0$ and $f_{\Lambda_b}^0$ are the fractions of B_s and Λ_b in the neutral b hadron sample. The P_s^Q values for B_s and Λ_b are given in an analogous way to equation 12 but with the factor $(1 - f_{\mathrm{B_s}}^0 - f_{\Lambda_b}^0)$ replaced by $f_{\mathrm{B_s}}^0$ or $f_{\Lambda_b}^0$. Finally the background function $P_{\mathrm{bg}}^Q(Q) = f_{\mathrm{bg}}$, *i.e.* the background fraction is a constant independent of Q, as found in Monte Carlo.

These functions together describe the source fractions as a function of Q in terms of four parameters: c_1 and c_2, which are left free in the fit; and c_0 and c_3, which are input from Monte Carlo. The values of c_1 and c_2 are constrained by the correlation between the type of b hadron in the M-tag hemisphere and the production flavour (b or $\bar{b}$) of the other b hadron in the T-tag hemisphere. The contamination of neutral b hadrons at $Q \approx \pm 1$ (which is given by $1 - c_1 - c_3$) is thus determined almost entirely from the data, whilst the contamination of charged b hadrons at $Q \approx 0$ (given by c_0) has to be taken from Monte Carlo, since the vertex charge provides no distinguishing power between neutral b and $\bar{b}$ hadrons.
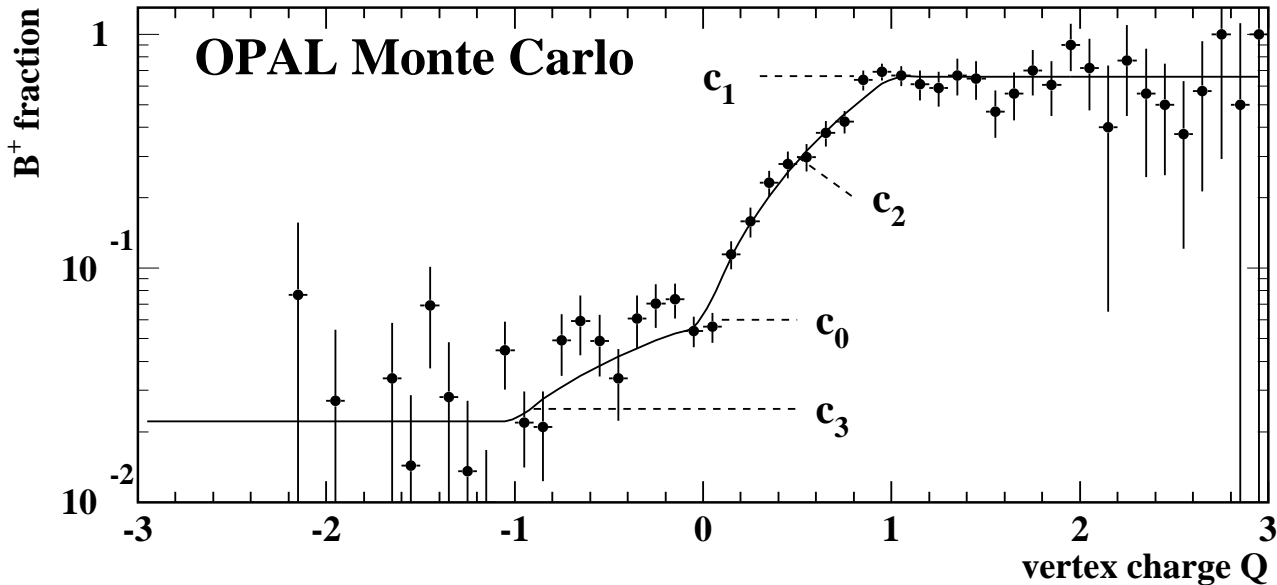
17

Figure 6: Fraction of B^+ vertices as a function of vertex charge Q in Monte Carlo $b\bar{b}$ events (points with error bars). The parameterisation is shown by the solid line, and the levels c_0, c_1 and c_3 by the dotted lines. The quadratic coefficient c_2 is used between $Q = 0$ and $Q = 1$. Note that the non-$b\bar{b}$ background fraction is not included, and the B^+ fraction is plotted using a logarithmic scale.

The function $P_s^T(Q_T)$ in equation 11 gives the probability for each source to be tagged by the opposite hemisphere flavour tag of value Q_T:

$$P_s^T(Q_T) = \begin{cases} (1 - Q_T)/2 & \text{for } s = B^+, B^0, B_s, \bar{\Lambda}_b \\ (1 + Q_T)/2 & \text{for } s = B^-, \bar{B}^0, \bar{B}_s, \Lambda_b \\ 1 & \text{for } s = \text{background} \end{cases}$$

Finally, the fractions f_s^j of each source contributing in each bin j of the time likelihood (equation 9) are given by the average of the source fractions f_s^i for each of the events i in bin j, where:

$$f_s^i = \frac{P_s^Q(Q_i) P_s^T(Q_{Ti})}{\sum_{s'} P_{s'}^Q(Q_i) P_{s'}^T(Q_{Ti})}$$

In total, 5 parameters were left free in the fit: the B^+ and B^0 lifetimes τ_{B+} and τ_{B^0}, the charge separation parameters c_1 and c_2, and the distortion parameter d. The B_s and Λ_b lifetimes were taken to be 1.54 ± 0.07 ps and 1.22 ± 0.05 ps [1]. The background lifetime was taken to be that in the Monte Carlo, $\tau_{bg} = 2.1$ ps, and the background fraction was measured to be $f_{bg} = 0.052 \pm 0.015$ (see Table 1). The remaining parameters $f_{B_s}^0$, $f_{\Lambda_b}^0$, c_0 and c_3 were taken from the Monte Carlo. Uncertainties on all these parameters are considered when evaluating the systematic errors.

The results of the fit for the B^+ and B^0 lifetimes are:

$$\tau_{B+} = 1.643 \pm 0.037 \text{ ps}$$
$$\tau_{B^0} = 1.523 \pm 0.057 \text{ ps}$$

where the errors are statistical only. The correlation coefficient between the two measured lifetimes is -0.53, and their ratio is $\tau_{B+}/\tau_{B^0} = 1.079 \pm 0.064$. The other fitted parameters were measured to be $c_1 = 0.84 \pm 0.03$, $c_2 = 0.10 \pm 0.18$ and $d = 1.76 \pm 0.21$ ps.

Source	$\Delta\tau_{B^+}$ (ps)	$\Delta\tau_{B^0}$ (ps)	$\Delta\tau_{B^+}/\tau_{B^0}$
B_s lifetime	0.000	0.026	0.019
b baryon lifetime	0.000	0.011	0.008
B_s/B^0 fraction	0.000	0.001	0.001
Λ_b/B^0 fraction	0.000	0.025	0.018
Background lifetime	0.005	0.009	0.003
Background fraction	0.010	0.015	0.004
Fit procedure	0.014	0.023	0.022
Charge separation	0.005	0.019	0.015
b fragmentation	0.008	0.009	0.000
Detector resolution	0.008	0.007	0.009
Silicon alignment	0.009	0.011	0.012
Total	0.025	0.053	0.041

Table 2: Systematic errors on the measured values of τ_{B^+}, τ_{B^0} and τ_{B^+}/τ_{B^0}. The values for τ_{B^+}/τ_{B^0} take into account correlations between τ_{B^+} and τ_{B^0}.

The distribution of mean excess decay time $\langle t \rangle$ as a function of $|Q|$ is shown in Figure 5, for data and for Monte Carlo simulation reweighted to the measured B^+ and B^0 lifetimes. The Monte Carlo sample is 13 times larger than the data sample, and the χ^2 between data and Monte Carlo distributions is 9.4 for 8 degrees of freedom. The results of the fit to the data (the values of τ_j) are shown by the dashed line, and the fit follows the data reasonably well. The distribution of data excess proper time in various regions of $|Q|$ is shown in Figure 7, again together with the reweighted Monte Carlo simulation. The deviations from a pure exponential away from integer values of Q can clearly be seen in both data and Monte Carlo.

6.4 Systematic errors

The systematic errors on the B^+ and B^0 lifetime measurements and their ratio are summarised in Table 2, and discussed in more detail below. In most cases, the systematic errors are evaluated by repeating the fit in either data or Monte Carlo, varying the appropriate parameter.

B_s and Λ_b contamination: The neutral b hadron sample consists not only of B^0 mesons but an irreducible contribution from B_s and Λ_b. Uncertainties in both the lifetimes (τ_{B_s} and τ_{Λ_b}) and sizes ($f^0_{B_s}$ and $f^0_{\Lambda_b}$) of these backgrounds affect the B^0 lifetime measurement, the B_s lifetime being the largest single source of uncertainty. The efficiencies for B^0, B_s and Λ_b to pass the vertex selection requirements are similar, but somewhat sensitive to their average charged decay multiplicities. However, by far the largest uncertainty in the level of contamination comes from the knowledge of the B_s and Λ_b production fractions in $Z^0 \rightarrow b\overline{b}$ events, taken to be $f(b \rightarrow B_s) = 10.5^{+1.8}_{-1.7}\,\%$ and $f(b \rightarrow \Lambda_b) = 10.1^{+3.9}_{-3.1}\,\%$ [1].

Non-b$\overline{b}$ background contamination: The effective mean decay time of the non-b$\overline{b}$ contamination in the selected sample is 2.1 ps in Monte Carlo. This has two distinct components—a contribution from mis-measured tracks and strange particle decays causing fake b decay vertices with long decay lengths, and a contribution from the decay of charm hadrons which have genuine lifetime. Charm events have both contributions, giving an effective lifetime of about 1.8 ps. Only the former contribution is present in uds events, which have an effective lifetime of about 2.3 ps.

To study the modelling of the background lifetime, two control samples were used, generated by modifying the selection for the T-tag. Requiring the vertex tag variable B in the T-tag to be between 0 and 1.2 gave a sample consisting of 9 % uds, 18 % c$\overline{c}$ and 72 % b$\overline{b}$ events, and requiring the T-tag hemisphere to fail the vertex tag pre-selection [23] gave a sample of 41 %
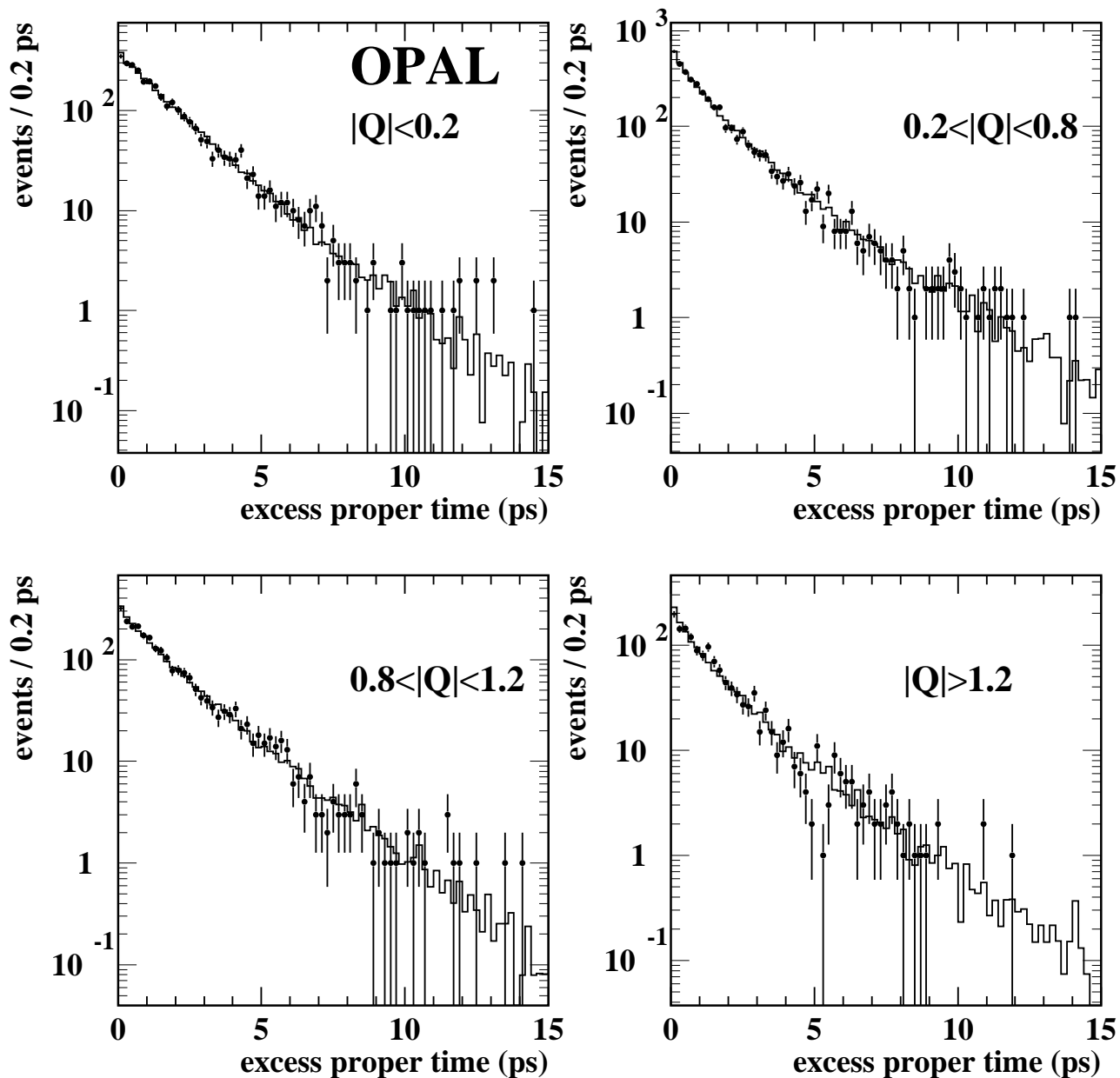
Figure 7: Distributions of excess proper time in four regions of absolute vertex charge $|Q|$, for data (points with error bars) and Monte Carlo simulation (histogram). The Monte Carlo B^+ and B^0 lifetimes have been reweighted to the same values as measured in the data.

uds, 23 % $c\bar{c}$ and 35 % $b\bar{b}$ events. The effective lifetimes measured in the M-tag hemispheres for these samples were found to agree in data and Monte Carlo to better than 0.05 ps. From this, an upper limit due to the mis-modelling of the background in the primary b-tagged sample was estimated as 0.1 ps, and used to assess the systematic error on the B^+ and B^0 lifetimes.

Fit procedure: The entire fitting procedure, including the derivation of the excess decay lengths and the correction for the distortion given in equation 10, was tested on a fully simulated Monte Carlo sample 13 times larger than the data sample. In this sample, where the B^+ and B^0 lifetimes were both 1.6 ps, the fit gave the results $\tau_{B^+} = 1.588 \pm 0.014$ ps and $\tau_{B^0} = 1.623 \pm 0.017$ ps. The larger of the deviations of these results from the true values or the statistical errors were taken as systematic errors due to the fitting procedure. As can be seen from Figures 5 and 7, the Monte Carlo provides a good description of the time distributions in the data.

Additional Monte Carlo studies were performed to check the correctness of the fit procedure and errors. To verify the errors returned by the fit, it was performed on many Monte Carlo subsamples, and the distribution of fitted lifetimes studied. The Monte Carlo was also reweighted to change the B^+ and B^0 lifetimes one at a time. In each case, the fit correctly recovered the modified lifetime, whilst returning a stable result for the lifetime of the unmodified b hadron.

As a cross check, the fit to the data was repeated with the parameterisation of the distortion given in equation 10 replaced with the distortions measured in the large Monte Carlo sample. Consistent results were obtained, with the values of τ_{B^+} and τ_{B^0} changing by 0.017 ps and -0.013 ps respectively.

Charge separation: The fraction of neutral b hadron contamination at $|Q| \approx 1$ (*i.e.* $1 - c_1 - c_3$) was fitted from the data. However, the corresponding contamination of charged b hadrons at $Q \approx 0$ (*i.e.* c_0), and the fraction of wrong sign charged b hadrons c_3 were taken from the Monte Carlo, and varied by ± 50 % to assess the systematic error (see Figure 6). This variation is larger than the difference seen between data and Monte Carlo in the neutral contamination of the charged b sample, and also larger than the variation resulting from changing the b hadron charged decay multiplicities within their experimental uncertainties [32].

The fit to determine the charge separation depends on the T-tag hemisphere production flavour tag Q_{T}, which is subject to mis-tag and jet and vertex charge offset subtraction uncertainties, as discussed in Section 5. The effect of these uncertainties on the b hadron lifetime measurement is negligible.

b fragmentation: The effect of uncertainties in the average b hadron energy $\langle x_E \rangle = E_{\text{b}}/E_{\text{beam}}$ was assessed in Monte Carlo by reweighting so as to vary $\langle x_E \rangle$ in the range 0.702 ± 0.008 [32], and repeating the lifetime fit. The effect on the lifetimes is small since the b hadron energy is estimated event by event.

Detector resolution and alignment: The error due to uncertainty in the tracking detector resolution was assessed in Monte Carlo by applying a global 10 % degradation to the resolution of all tracks, independently in the r-ϕ and r-z planes, as in [23]. The lifetime measurements are also sensitive to the effective radial positions of the silicon detectors (both the positions of the detectors themselves and the positions of the charge collection regions within them). These are known to a precision of $\pm 20\,\mu$m from studies of cosmic ray events [23]. The resulting uncertainty was calculated by applying $20\,\mu$m radial shifts to one or both silicon layers in Monte Carlo and repeating the lifetime fits.

The total systematic errors amount to ± 0.025 ps on the B^+ and ± 0.053 ps on the B^0 lifetimes, and ± 0.041 on their ratio, where correlated systematic errors have been taken into account.

7 CP(T) violation analysis

In the Standard Model framework for describing CP violation, according to the formalism given in equation 1, an asymmetry is predicted in the time dependent inclusive decay rates of B^0 and $\bar{B}^0$ mesons:

$$A(t') \equiv \frac{\Gamma(B^0 \rightarrow \text{anything}) - \Gamma(\bar{B}^0 \rightarrow \text{anything})}{\Gamma(B^0 \rightarrow \text{anything}) + \Gamma(\bar{B}^0 \rightarrow \text{anything})}$$

For a totally unbiased selection of B^0 and $\bar{B}^0$ mesons, the form of this asymmetry as a function of true proper decay time t' is given by:

$$A(t') = a_{\rm cp} \left\{ \frac{\Delta m_{\rm d} \tau_{B^0}}{2} \sin(\Delta m_{\rm d} t') - \sin^2 \left(\frac{\Delta m_{\rm d} t'}{2} \right) \right\} \tag{13}$$

where $a_{\rm cp}$ is the CP-violating observable, $\Delta m_{\rm d}$ is the B^0 oscillation frequency and τ_{B^0} the B^0 lifetime [12,33]. The parameter $a_{\rm cp}$ is related to the CP-violation parameter $\epsilon_{\rm B}$ by:

$$\mathrm{Re}(\epsilon_{\rm B}) = \frac{a_{\rm cp}}{4} \tag{14}$$

using the convention that $|\epsilon_{\rm B}|$ is small. Searching for an asymmetry of the form given in equation 13 therefore provides a method of probing the value of $\epsilon_{\rm B}$. In the Standard Model, $\mathrm{Re}(\epsilon_{\rm B})$ is expected to be around 10^{-3} [12], but it could be up to an order of magnitude larger in superweak models [34].

In this analysis, the T-tag is used to tag $b\bar{b}$ events, and an inclusive reconstruction algorithm is used to reconstruct the b hadron decay time t in the M-tag hemisphere. The production flavour (b or $\bar{b}$) of this M-tagged b hadron is given by the combined tagging variable Q_2 (see section 5), using information from both hemispheres of the event. No attempt is made to separate B^0 and $\bar{B}^0$ decays from other b hadron decays in the M-tag hemisphere. A similar asymmetry to that given in equation 13 is expected for $B_{\rm s}$ mesons, with $\Delta m_{\rm d}$ replaced with the $B_{\rm s}$ oscillation frequency $\Delta m_{\rm s}$, but it is expected to be at least an order of magnitude smaller and is neglected. No asymmetry is expected for B^+ and $\Lambda_{\rm b}$. These other b hadrons therefore dilute the expected B^0 asymmetry, but do not change its form. Hence no attempt is made to remove B^+ decays by requiring well reconstructed neutral vertices, as this would not greatly increase the sensitivity to CP violation in the B^0 decays, and would lead to a large loss in reconstruction efficiency.

Although the time dependent rates of B^0 and $\bar{B}^0$ decay are predicted to be different, this does not violate the CPT invariance prediction of equal total decay rates. The lifetimes of B^0 and $\bar{B}^0$ are thus still expected to be equal. If CPT violation were present, the lifetimes of b and $\bar{b}$ hadrons could be different:

$$
\begin{aligned}
\tau_{\rm b} &= \left\{ 1 + \frac{1}{2} \left(\frac{\Delta \tau}{\tau} \right)_{\rm b} \right\} \tau_{\rm av} \\
\tau_{\bar{\rm b}} &= \left\{ 1 - \frac{1}{2} \left(\frac{\Delta \tau}{\tau} \right)_{\rm b} \right\} \tau_{\rm av}
\end{aligned}
\tag{15}
$$

where $\tau_{\rm av}$ is the average and $(\Delta \tau / \tau)_{\rm b}$ the fractional difference in lifetimes. The value of $(\Delta \tau / \tau)_{\rm b}$ is determined by measuring the lifetimes of b and $\bar{b}$ hadrons, using the same time reconstruction algorithm as for the CP-violation analysis.

7.1 b hadron reconstruction

The b hadron decay length was reconstructed using a secondary vertex finding algorithm similar to those employed in [28] and [31]. In the highest energy jet in the M-tag hemisphere, the two tracks with the largest impact parameter with respect to the primary vertex were used to form a 'seed' vertex. All tracks consistent with this seed vertex were then added to it using an iterative procedure. Only

tracks satisfying the quality requirements detailed in Section 6.1 were considered for inclusion in the secondary vertex.

The resulting vertex was required to have at least three tracks, and the invariant mass (assuming all tracks to be pions) was required to be at least $0.8\,\mathrm{GeV}$. The transverse miss distance (the projection of the vector between primary and secondary vertices onto a plane orthogonal to the total momentum vector of the tracks assigned to the secondary vertex) divided by its error was required to be less than 3 [31]. These requirements help to eliminate badly reconstructed and fake secondary vertices. The decay length L between primary and secondary vertices was then calculated, using the jet axis direction as a constraint, as in [23]. An acceptable secondary vertex was found in approximately $70\,\%$ of hemispheres, for both $b\bar{b}$ and background ($c\bar{c}$ and light quark) events.

The b hadron energy was estimated as described in section 6.2, calculating the charged fragmentation energy using weights w_i tuned with this alternative vertex finder. The estimate t of the b hadron decay proper time was then calculated as before:

$$t = \frac{m_{\mathrm{b}} L}{\sqrt{E_{\mathrm{b}}^2 - m_{\mathrm{b}}^2}} \; .$$

In Monte Carlo, the resolution of this estimate can be described by the sum of two Gaussians. For the 1993–95 data, the narrower Gaussian has an RMS width of $0.33\,\mathrm{ps}$ and contains $65\,\%$ of the events, and the wider Gaussian has a width of $1.3\,\mathrm{ps}$. For the 1991–92 data, where the vertex reconstruction was done in the r-ϕ plane only, the narrow Gaussian has a width of $0.33\,\mathrm{ps}$ and contains $64\,\%$ of events, and the wider Gaussian has a width of $1.4\,\mathrm{ps}$. Since the resolutions are similar, the two data samples were combined and a single resolution function used for the entire sample. These resolutions are an average over all true decay proper times t', and significant non-Gaussian effects can be seen in small slices of t', as in [31]. These effects are caused by the presence of tracks from the primary vertex, and make a full description of the resolution as a function of t' very complicated. However, they are not important for the analysis described here, which does not rely heavily on an accurate description of the decay time resolution.

7.2 Fit and results for $\epsilon_{\mathbf{B}}$

The CP-violating parameter a_{cp} was extracted using a χ^2 fit to the observed time dependent asymmetry $A(t)$ in 34 bins of reconstructed time in the range -2 to $15\,\mathrm{ps}$. Within each time bin i, the observed asymmetry was calculated in ten bins j of $|Q_2|$ ($0 < |Q_2| < 1$) to make best use of the tagging information in each event. These ten estimates of the asymmetry were averaged with appropriate weights to calculate the overall observed asymmetry A_i^{obs} in each time bin i. The observed asymmetry was compared with the expected asymmetry A_i^{true} calculated for a given a_{cp}, taking into account the time resolution and dilution from non-B^0 decays in the event sample.

The corrected observed asymmetry in bin i of reconstructed time t and bin j of $|Q_2|$ is given by:

$$A_{ij}^{\mathrm{obs}} = \frac{N_{ij}^{\mathrm{b}} - N_{ij}^{\bar{\mathrm{b}}}}{\langle |Q_2| \rangle_{ij} (N_{ij}^{\mathrm{b}} + N_{ij}^{\bar{\mathrm{b}}})}$$

and the error $\sigma_{A_{ij}^{\mathrm{obs}}}$ is given by:

$$\sigma_{A_{ij}^{\mathrm{obs}}} = \frac{1 - (\langle |Q_2| \rangle_{ij} A_{ij}^{\mathrm{obs}})^2}{2 \langle |Q_2| \rangle_{ij}} \sqrt{\frac{N_{ij}^{\mathrm{b}} + N_{ij}^{\bar{\mathrm{b}}}}{N_{ij}^{\mathrm{b}} N_{ij}^{\bar{\mathrm{b}}}}}$$

where N_{ij}^{b} ($N_{ij}^{\bar{\mathrm{b}}}$) is the number of events with $Q_2 > 0$ ($Q_2 < 0$). The factor $1/\langle |Q_2| \rangle_{ij}$ corrects for the tagging dilution (mis-tagging), which reduces the observed asymmetry for imperfectly tagged events.
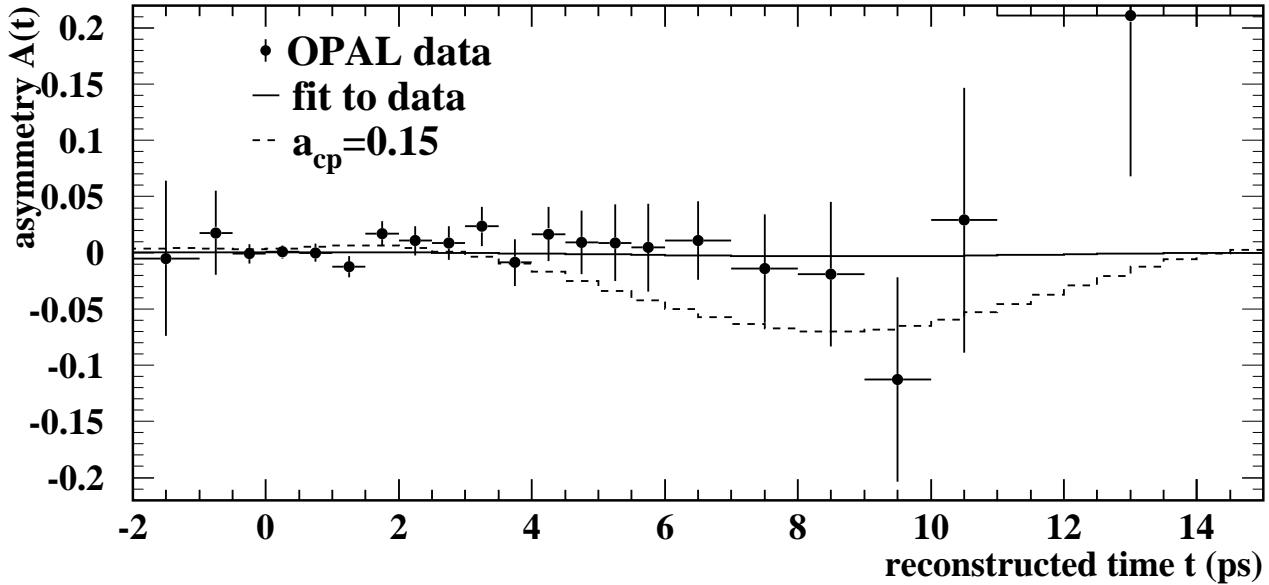
Figure 8: Asymmetry of tagged b and $\overline{\text{b}}$ hadrons as a function of reconstructed time t in data (points), and fit (solid line). The expected asymmetry for $a_{\text{cp}} = 0.15$ is shown by the dotted line.

The ten estimates A_{ij}^{obs} were then averaged, weighting according to $(\sigma_{A_{ij}^{\text{obs}}})^{-2}$ to derive the corrected observed asymmetry A_i^{obs}.

The true asymmetry as a function of reconstructed time t is given by:

$$A^{\text{true}}(t) = (1 - f_{\text{bg}})f_{\text{B}^0} \left\{ \frac{\int_0^\infty P(t)A(t')R(t-t')dt'}{\int_0^\infty P(t)R(t-t')dt'} \right\}$$

where f_{bg} is the fraction of non-b$\overline{\text{b}}$ events in the sample, f_{B^0} is the fraction of B^0 in the b$\overline{\text{b}}$ part of the sample, $P(t')$ is the lifetime exponential $P(t') = (1/\tau_{\text{B}^0})e^{-t'/\tau_{\text{B}^0}}$, $A(t')$ is the asymmetry as a function of true proper time t' given in equation 13, and $R(t - t')$ is the time resolution function. $R(t')$ is the sum of two Gaussians, with parameters given in section 7.1. The expected asymmetry in time bin i was calculated from the mean reconstructed decay time of all events in bin i: $A_i^{\text{true}} = A^{\text{true}}(\langle t \rangle_i)$.

A binned χ^2 fit was performed to the distribution of asymmetry as a function of reconstructed time. Both 1991–92 and 1993–95 data samples were used together, setting the background parameter to the average impurity of the two samples, $f_{\text{bg}} = 13.7 \pm 3.0\,\%$ (see Table 1). The values of τ_{B^0} and Δm_{d} were taken to be $\tau_{\text{B}^0} = 1.56 \pm 0.04\,\text{ps}$ and $\Delta m_{\text{d}} = 0.464 \pm 0.018\,\text{ps}^{-1}$ [1]. The parameter f_{B^0} was taken from the Monte Carlo to be $f_{\text{B}^0} = 0.41$.

The observed asymmetry for the 394 119 data events is shown in Figure 8, together with the result of the one parameter fit to a_{cp}. The fit result is

$$a_{\text{cp}} = 0.005 \pm 0.055$$

where the error is statistical only.

The form of the asymmetry given in equation 13 assumes that the reconstruction efficiencies for all decay modes are equal. In particular, if the efficiency to reconstruct B^0 decays to final states containing no charm hadron, one charm hadron and two charm hadrons are different, then additional asymmetries may be seen [33]. This is because the semi-inclusive B^0 decays to final states containing

Source	Δa_{cp}	Δc_{cp}
B^0 lifetime	0.002	0.000
Δm_{d} value	0.001	0.001
B^0 fraction	0.002	0.002
Flavour tagging offsets	0.003	0.013
Flavour tagging mis-tag	0.009	0.005
b fragmentation	0.008	0.006
Time resolution	0.002	0.000
Total	0.013	0.015

Table 3: Systematic errors on the measured values of a_{cp} (from the one parameter fit) and c_{cp} (from the two parameter fit).

different numbers of charm hadrons may exhibit larger CP-violating effects of different signs which largely cancel out in the inclusive decay. In this case, the expected asymmetry takes the form

$$A(t') = c_{\mathrm{cp}} \sin(\Delta m_{\mathrm{d}} t') - a_{\mathrm{cp}} \sin^2 \left(\frac{\Delta m_{\mathrm{d}} t'}{2} \right) \qquad (16)$$

where a_{cp} is still related to $\mathrm{Re}(\epsilon_{\mathrm{B}})$ as in equation 14, and c_{cp} is an additional CP-violating parameter [33]. A second fit to the form shown in equation 16, allowing the values of both a_{cp} and c_{cp} to vary, gave the results

$$
\begin{aligned}
a_{\mathrm{cp}} &= 0.002 \pm 0.055 \\
c_{\mathrm{cp}} &= 0.026 \pm 0.027
\end{aligned}
$$

where again the errors are statistical only, and the correlation coefficient between the two parameters is 0.72. No evidence is seen for a significant $\sin(\Delta m_{\mathrm{d}} t')$ term, and the value of a_{cp} shifts by only -0.003 (5 % of the statistical error) with respect to the one parameter fit, showing that the effects of efficiency differences are not significant.

The systematic errors on the values of a_{cp} and c_{cp} (from the one and two parameter fits respectively) are all small compared to the statistical errors. They are shown in Table 3, and discussed in more detail below.

Physics input parameters: The values of the B^0 lifetime τ_{B^0} and oscillation frequency Δm_{d} were taken from [1] and varied within the quoted errors.

B^0 fraction: The fraction of B^0 events in the data sample depends on the production fractions of B_{s} and Λ_{b} in $b\overline{b}$ events [1] and on the fraction of non-$b\overline{b}$ background, determined to be 13.7 ± 3.0 % from the data.

Flavour tagging: The offsets in the jet and vertex charges used for tagging the B^0 production flavour were measured directly in the data, as described in Section 5. The uncertainties in these offsets contribute to the systematic errors on a_{cp} and c_{cp}.

If a time dependent CP-violating effect were present, it could change the value of the offset measured for the T-tag vertex charge Q_{vtx}, as the vertex tagged sample (being biased towards long B^0 decay times) would contain an unequal mixture of B^0 and $\bar{B}^0$ which do not have equal vertex charge offsets. With the offsets measured in Monte Carlo and a CP-violating effect of $a_{\mathrm{cp}} = 0.05$, this effect would shift the Q_{vtx} offset by 0.0006 of the RMS width of the Q_{vtx} distribution. This shift is much smaller than the statistical error on the vertex charge offset in the data, and does not present an important additional source of systematic error.

The production flavour mis-tag probabilities as a function of Q_T and Q_M were also tested in the data, and found to be correct to precisions of 2.6 % and 10 %, respectively (see Section 5). These uncertainties were translated into errors on a_{cp} and c_{cp} by scaling the values of Q_T and Q_M by ± 2.6 % and ± 10 % as in [27] and repeating the fits.

Reconstruction asymmetry: The fit assumes that the secondary vertex reconstruction efficiencies in the M-tag hemisphere are equal for B^0 and $\bar{B}^0$ mesons. The track reconstruction asymmetries mentioned in section 5 may potentially introduce an efficiency asymmetry, since the vertex reconstruction requires a secondary vertex with at least three tracks, and the sign of the highest momentum tracks will be different for B^0 and $\bar{B}^0$ mesons. However, the track reconstruction asymmetries in the Monte Carlo, which are somewhat larger than those in the data, lead to no significant efficiency asymmetry for reconstructing secondary vertices.

b fragmentation: The proper time reconstruction depends slightly on the average energy of the b hadrons. This effect was assessed by reweighting Monte Carlo events and repeating the fit, as discussed in Section 6.4.

Time resolution: The fit is rather insensitive to the reconstructed proper time resolution, since the effects of CP violation are characterised by a time scale $t \approx \pi / \Delta m_d$ which is much larger than the average proper time resolution. The sensitivity was assessed by varying the width of each Gaussian in the resolution function by ± 10 %, varying the fraction of the wider Gaussian by ± 50 % and by using an alternative resolution function parameterisation derived from a Monte Carlo sample with 10 % degraded tracking resolution, as in Section 6.4.

The fit was tested on Monte Carlo by introducing non-zero values of a_{cp} and c_{cp}, and checking that the fit correctly reproduced the input asymmetries. The fit errors were also verified to be correct by splitting the Monte Carlo input into several sub-samples and studying the distributions of fitted outputs.

Including all systematic errors, the value of a_{cp} was determined from the one parameter fit to be $a_{cp} = 0.005 \pm 0.055 \pm 0.013$. The value of c_{cp} was determined from the two parameter fit to be $c_{cp} = 0.026 \pm 0.027 \pm 0.015$. The result for a_{cp} can be translated into a measurement of $\mathrm{Re}(\epsilon_B)$ using equation 14, and gives

$$\mathrm{Re}(\epsilon_B) = 0.001 \pm 0.014 \pm 0.003$$

where the first error is statistical and the second systematic.

7.3 Fit and results for $(\Delta\tau/\tau)_b$

The same data sample was used to measure the fractional difference between b and $\bar{b}$ hadron lifetimes. This was done by dividing the data into 20 bins of $b/\bar{b}$ hadron purity using the tagging variable Q_2 and simultaneously fitting all the reconstructed proper time distributions. The expected proper time distribution $F_j(t)$ in bin j of the tagging variable Q_2 ($-1 < Q_2 < 1$) is given by:

$$F_j(t) = \int_0^\infty P_j(t')R(t-t')dt'$$

where $P(t')$ describes the true proper time distribution of the events and $R(t-t')$ is the time resolution function. The true proper time distribution is given by:

$$P_j(t') = (1-f_{bg})\left\{\frac{(1+\langle Q_2\rangle_j)}{2}\frac{1}{\tau_b}e^{-t'/\tau_b} + \frac{(1-\langle Q_2\rangle_j)}{2}\frac{1}{\tau_{\bar{b}}}e^{-t'/\tau_{\bar{b}}}\right\} + f_{bg}\left\{f_\delta\,\delta(t') + (1-f_\delta)\frac{1}{\tau_{bg}}e^{-t'/\tau_{bg}}\right\}$$

where f_{bg} is the fraction of non-$b\bar{b}$ background in the data sample and $\langle Q_2\rangle_j$ is the average value of Q_2 in the tagging bin j. The parameters τ_b and $\tau_{\bar{b}}$ are the lifetimes of b and $\bar{b}$ hadrons, related to the

Source	$\Delta((\Delta\tau/\tau)_{\mathrm{b}})$
Background fraction	0.000
Background lifetime	0.000
Flavour tagging offsets	0.001
Flavour tagging mis-tag	0.008
b fragmentation	0.000
Time resolution	0.001
Total	0.008

Table 4:   Systematic errors on the measured value of $(\Delta\tau/\tau)_{\mathrm{b}}$.

average lifetime τ_{av} and fractional difference $(\Delta\tau/\tau)_{\mathrm{b}}$ by equation 15. The non-$\mathrm{b\overline{b}}$ background was modelled by two components—a fraction f_δ at $t' = 0$ and the remainder having a lifetime τ_{bg}, both distributions being convolved with the same resolution function as the signal.

A two parameter χ^2 fit was performed to the 20 reconstructed proper time distributions in $0.5\,\mathrm{ps}$ bins between 1 and $15\,\mathrm{ps}$, fitting the values of $(\Delta\tau/\tau)_{\mathrm{b}}$ and τ_{av}. The region below $1\,\mathrm{ps}$ was excluded from the fit because the function $F_j(t)$ does not give a good representation of the data in this region. This is because of the effects of the primary vertex on the resolution function $R(t - t')$ discussed in Section 7.1. Such effects have to be taken into account when fitting the lifetime itself [31], but are not important when searching for a difference in b and $\overline{\mathrm{b}}$ hadron lifetimes.

In the fit, the background fraction was set to $f_{\mathrm{bg}} = 13.4 \pm 3.0\,\%$ as in Section 7.2. The background parameters were taken from the Monte Carlo and set to $f_\delta = 0.87$ and $\tau_{\mathrm{bg}} = 2.9\,\mathrm{ps}$.

The results of the fit were

$$\left(\frac{\Delta\tau}{\tau}\right)_{\mathrm{b}} = -0.001 \pm 0.012$$

and $\tau_{\mathrm{av}} = 1.500 \pm 0.003\,\mathrm{ps}$, where the errors are statistical only. The result for τ_{av} has large systematic errors of the order of $0.1\,\mathrm{ps}$ associated with the resolution function and should not be interpreted as a measurement of the average b hadron lifetime.

The distributions of proper time in four different ranges of Q_2, together with the fit results and expectation for $(\Delta\tau/\tau)_{\mathrm{b}} = 0.2$, are shown in Figure 9. The fit describes the data well, and no evidence for a difference between b and $\overline{\mathrm{b}}$ hadron lifetimes is seen.

The systematic errors on $(\Delta\tau/\tau)_{\mathrm{b}}$ are small, as most uncertainties affect both lifetimes in the same way. They are summarised in Table 4. Most of them are similar to those of the CP-violation analysis described in Section 7.2, and were evaluated in the same way. The uncertainty from the background lifetime was evaluated by varying the fraction of background at $t' = 0$ from $82\,\%$ to $92\,\%$, and by varying the lifetime of the other component from $2.4\,\mathrm{ps}$ to $3.4\,\mathrm{ps}$. No significant effect was seen.

The total systematic error on $(\Delta\tau/\tau)_{\mathrm{b}}$ is ± 0.008, and is dominated by the uncertainty on the flavour mis-tag rates. Additionally, it was checked that the fit was stable with respect to variations of the minimum and maximum time cuts. The fit was tested on Monte Carlo by reweighting so as to introduce variations between the b and $\overline{\mathrm{b}}$ hadron lifetimes, and checking that the fit recovered the correct values of $(\Delta\tau/\tau)_{\mathrm{b}}$. The errors were checked by splitting the Monte Carlo into subsamples, as before.
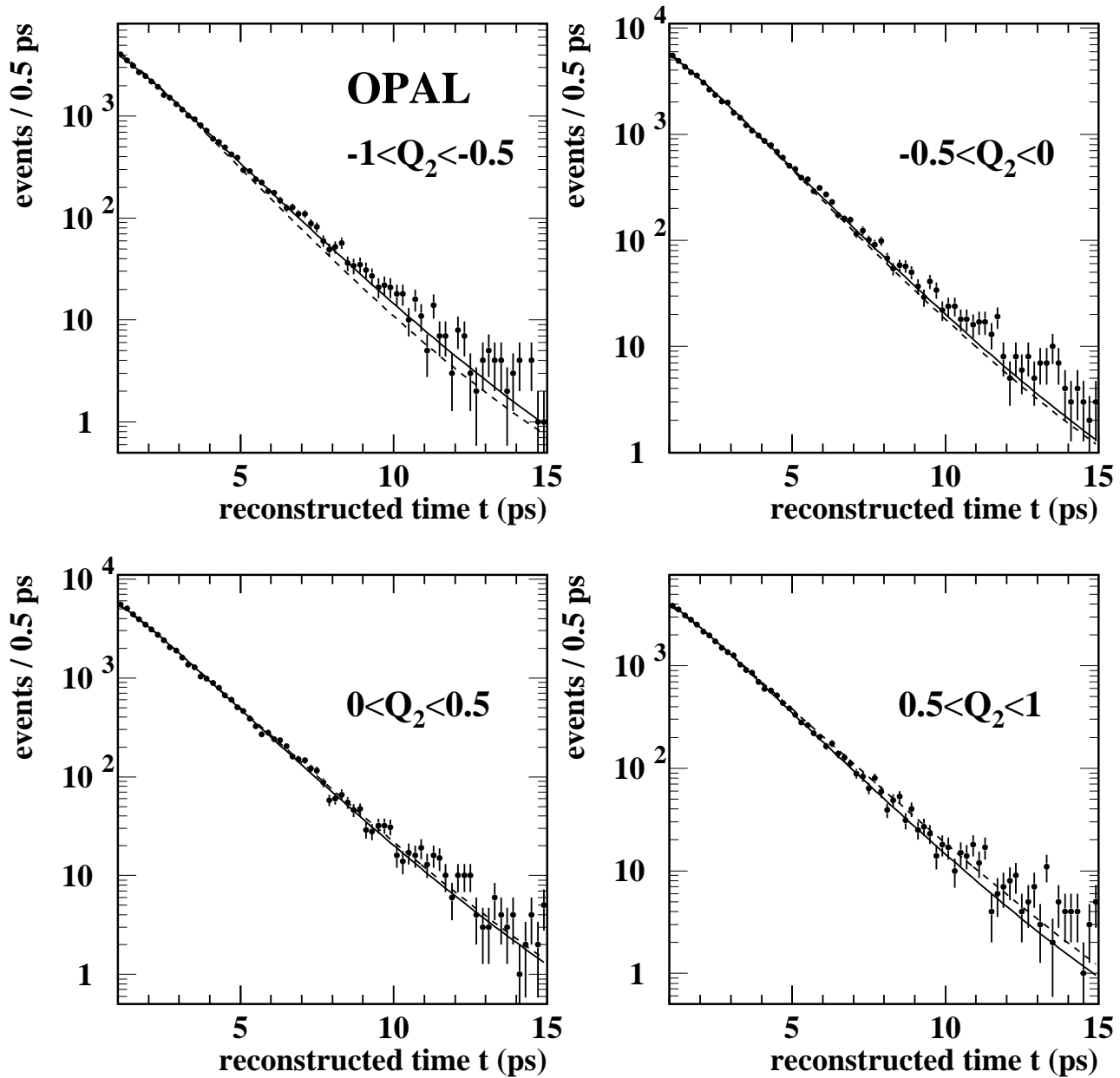
Figure 9: Distributions of reconstructed proper time t ($1 < t < 15\,\mathrm{ps}$) in four bins of tag variable Q_2. The data are shown by the points with error bars, and the prediction of the fit by the solid lines. The expected distributions for a $20\,\%$ difference between b and $\overline{\mathrm{b}}$ hadron lifetimes ($(\Delta\tau/\tau)_{\mathrm{b}} = 0.2$) are shown by the dotted lines.

8 Summary and conclusions

The lifetimes of the B^+ and B^0 mesons, and their ratio, have been measured using a technique based on reconstructed secondary vertices. From a sample of 2 390 221 hadronic Z^0 decays collected by the OPAL detector between 1993 and 1995, the results

$$
\begin{aligned}
\tau_{B^+} &= 1.643 \pm 0.037 \pm 0.025 \,\mathrm{ps} \\
\tau_{B^0} &= 1.523 \pm 0.057 \pm 0.053 \,\mathrm{ps} \\
\tau_{B^+}/\tau_{B^0} &= 1.079 \pm 0.064 \pm 0.041
\end{aligned}
$$

were obtained, where in each case the first error is statistical and the second systematic. These results are in agreement with other measurements from LEP, SLD and CDF [3–6], and with the world average values of $\tau_{B^+} = 1.65 \pm 0.04 \,\mathrm{ps}$ and $\tau_{B^0} = 1.56 \pm 0.04 \,\mathrm{ps}$ [1]. The result for the B^+ lifetime is the most precise determination to date.

Using a similar technique, an inclusive sample of b hadron decays has been used to search for CP and CPT violation effects. No such effects have been seen. From the time dependent asymmetry of inclusive B^0 decays, the CP violation parameter has been determined to be

$$
\mathrm{Re}(\epsilon_B) = 0.001 \pm 0.014 \pm 0.003 \ .
$$

This result agrees with the OPAL measurement using semileptonic b decays: $\mathrm{Re}(\epsilon_B) = 0.002 \pm 0.007 \pm 0.003$ [10], and is also in agreement with other less precise results from CLEO and CDF [9].

The fractional difference in the lifetimes of b and $\overline{\mathrm{b}}$ hadrons has also been measured to be

$$
\left(\frac{\Delta\tau}{\tau}\right)_{\mathrm{b}} \equiv \frac{\tau(\mathrm{b\ hadron}) - \tau(\overline{\mathrm{b}}\ \mathrm{hadron})}{\tau(\mathrm{average})} = -0.001 \pm 0.012 \pm 0.008 \ .
$$

This is the first published analysis to test the equality of the b and $\overline{\mathrm{b}}$ hadron lifetimes.

References

[1] Particle Data Group, C. Caso et al., Eur. Phys. J. C3 (1998) 1.

[2] For example:
G. Alterelli and S. Petrarca, Phys. Lett. B261 (1991) 303;
I. Bigi, Phys. Lett. B169 (1986) 191;
I. Bigi and N.G. Uraltsev, Phys. Lett. B280 (1992) 271;
M. Neubert and C.T. Sachrajda, Nucl. Phys. B483 (1997) 339.

[3] OPAL collaboration, R. Akers et al., Z. Phys. C67 (1995) 379.

[4] ALEPH collaboration, D. Buskulic et al., Z. Phys. C71 (1996) 31;
CDF collaboration, F. Abe et al., Phys. Rev. Lett. 76 (1996) 4462;
CDF collaboration, F. Abe et al., Phys. Rev. D58 (1998) 092002;
DELPHI collaboration, P. Abreu et al., Z. Phys. C68 (1995) 13;
DELPHI collaboration, P. Abreu et al., Z. Phys. C74 (1997) 19.

[5] DELPHI collaboration, W. Adam et al., Z. Phys. C68 (1995) 363.

[6] SLD collaboration, K. Abe et al., Phys. Rev. Lett. 79 (1997) 590;
L3 collaboration, M. Acciarri et al., 'Upper Limit on the Lifetime Difference of Short- and Long-Lived B_s Mesons', CERN-EP/98-127, accepted by Phys. Lett. B.

[7] V.A. Kostelecky and R. Potting, Phys. Rev. D51 (1995) 3923.

[8] V.A. Kostelecky and R. Van Kooten, Phys. Rev. D54 (1996) 5585.

[9] CLEO collaboration, J. Bartelt et al., Phys. Rev. Lett. 71 (1993) 1680;
CDF collaboration, F. Abe et al., Phys. Rev. D55 (1997) 2546.

[10] OPAL collaboration, K. Ackerstaff et al., Z. Phys. C76 (1997) 401.

[11] For example: R. Hawkings, 'CP violation in B decays at LEP', talk presented at the 3rd International Conference on Hyperons, Charm and Beauty Hadrons, 2nd July 1998, Genova, Italy, to be published in Nucl. Phys. B.

[12] A. Acuto and D. Cocolicchio, Phys. Rev. D47 (1993) 3945;
M. Beneke, G. Buchalla and I. Dunietz, Phys. Lett. B393 (1997) 132.

[13] NA 14/2 collaboration, M.P. Alvarez et al., Z. Phys. C47 (1990) 539.

[14] OPAL collaboration, K. Ahmet et al., Nucl. Instrum. Methods A305 (1991) 275.

[15] P.P. Allport et al., Nucl. Instrum. Methods A324 (1993) 34.

[16] P.P. Allport et al., Nucl. Instrum. Methods A346 (1994) 476.

[17] OPAL collaboration, G. Alexander et al., Z. Phys. C52 (1991) 175.

[18] OPAL collaboration, R. Akers et al., Z. Phys. C63 (1994) 197.

[19] T. Sjöstrand, Comp. Phys. Comm. 82 (1994) 74.

[20] OPAL collaboration, G. Alexander et al., Z. Phys. C69 (1996) 543.

[21] C. Peterson, D. Schlatter, I. Schmitt and P. Zerwas, Phys. Rev. D27 (1983) 105.

[22] J. Allison et al., Nucl. Instrum. Methods A317 (1992) 47.

[23] OPAL collaboration, G. Abbiendi et al., 'A Measurement of $R_{\rm b}$ using a Double Tagging Method', CERN-EP/98-137, accepted by Eur. Phys. J. C.

[24] OPAL collaboration, G. Alexander et al., Z. Phys. C70 (1996) 357.

[25] OPAL collaboration, P.D. Acton et al., Z. Phys. C58 (1993) 523.

[26] OPAL collaboration, R. Akers et al., Z. Phys. C66 (1995) 555.

[27] OPAL collaboration, K. Ackerstaff et al., Eur. Phys. J. C5 (1998) 379.

[28] OPAL collaboration, R. Akers et al., Z. Phys. C66 (1995) 19.

[29] OPAL collaboration, R. Akers et al., Phys. Lett. B327 (1994) 411.

[30] OPAL collaboration, P.D. Acton et al., Z. Phys. C59 (1993) 183;
OPAL collaboration, R. Akers et al., Phys. Lett. B338 (1994) 497.

[31] OPAL collaboration, K. Ackerstaff et al., Z. Phys. C73 (1997) 397.

[32] The LEP experiments, ALEPH, DELPHI, L3 and OPAL, Nucl. Instrum. Methods A378 (1996) 101.
Updated averages are described in 'Presentation of LEP Electroweak Heavy Flavour Results for Summer 1998 Conferences', LEPHF 98-01 (see `http://www.cern.ch/LEPEWWG/heavy/`).

[33] I. Dunietz, 'CP Asymmetries in Semi-inclusive B^0 Decays', 30th June 1998, FERMILAB-PUB-97/323-T, hep-ph/9806521.

[34] D. Cocolicchio and L. Maiani, Phys. Lett. B291 (1992) 155;
J. Gerard and T. Nakada, Phys. Lett. B261 (1991) 474;
J. Liu and L. Wolfenstein, Phys. Lett. B197 (1987) 536.